SHAKE AND WAKE: INVESTIGATING HOW EARTHQUAKES TRIGGER VOLCANIC ACTIVITY BY SHAKING BUBBLES IN VISCOELASTIC FLUIDS AS AN ANALOGUE FOR MAGMA CHAMBERS DURING EARTHQUAKES

A thesis

submitted in partial fulfilment of the requirements for the Degree of

Master of Science in Geology

in the

University of Canterbury

by

Kaylon Higginbotham

Contents

1. Abstract

Shaking bubbles within a viscoelastic magma analogue material provides insight into how seismic shaking affects magma bodies. Volcanic eruptions connected to earthquakes have been recorded since the 19th Century and have been the focus of numerous studies. Anecdotal evidence, statistical studies, and numerical modelling indicate that both near- and far-field earthquakes can trigger volcanic activity. However, little experimental work has been done to constrain the dynamic interaction between the seismic trigger and the bubbly magma. Bubbles were injected into homogenous, silicon oil with a shear thinning rheology in a sealed tank and then subjected to shaking. The viscosities of the fluids tested were 2,000 Pa s, 10,000 Pa s, and 30,000 Pa s, simulating different magmas. Duration (s), displacement (mm), and frequency (Hz) of shaking were varied and the rate of bubble rise measured and bubble deformation recorded. Results indicate that bubble rise rate is affected by shaking exceeding accelerations over 0.5 *g* during which bubble rise rate increased by 1.91 % to 13.33 %. A positive correlation exists between increasing rise rate and higher acceleration of shaking. Viscosity, bubble size, and displacement of shaking do not appear to directly affect bubble rise rate. Duration affects bubble rise rate as the rise rate increase occurs only during shaking. Measured increase in rise of bubbles has implications for advective pressure increases and outgassing of magma following earthquakes. Rheology data for the viscoelastic fluid indicates that at the strain rates of the experiments some shear thinning behaviour could be expected to lower the measured viscosity, which may be reflected in the increased rise rates of bubbles. During shaking bubble shear was measured as bubbles became slightly deformed by dominantly simple shear and contraction. Higher accelerations in our Newtonian fluids result in a greater range and maximum value of shear strain. This gives rise to a capillary number allowing bubbles to deform. Fluid dynamics offer additional explanations for an increase in bubble rise rate associated with asymmetric bubbles such as a net lift that develops associated with lateral fluid flow around asymmetric bubbles, similar to aircraft wings, which promotes upward movement of bubbles. Therefore, bubble shear, combined with lowered viscosity due to the shear strain rate viscosity dependence of the fluids, may be mechanisms driving increased bubble migration during shaking.

Keywords: volcanic triggering, seismic triggering, dynamic triggering, bubble rise

2. Introduction

Volcanic activity triggered by earthquakes is an acknowledged but poorly understood phenomenon. Seismic activity has long been connected with volcanism, typically associated with the mobilization of fluids or magma and mass relocation (Unglert & Jellinek, 2015; Sánchez & McNutt, 2004). However, earthquakes triggering volcanic activity and eruptions is less often considered (Hill et al., 2002). Volcanic systems have previously been considered as primarily isolated systems, but this view has been shifting as new research is being carried out into volcano-tectonic connectivity (e.g. Eggert & Walter, 2009; Walter & Amelung, 2006).

Volcanic eruptions following earthquakes have been recorded in literature since as early as 1840 and has been the focus of many studies since then (e.g. Hill et al., 2002; Manga & Brodsky, 2006; Linde et al., 1994; Eggert & Walter, 2009). This has led to the assumption that both far-field and near-field earthquakes may trigger activity and eruptions in volcanoes (Manga & Brodsky, 2006). Volcanic triggering has been examined in case studies and by statistical analysis in order to substantiate the connection between earthquakes and triggered eruptions (e.g. Bebbington & Marzocchi, 2011; Linde et al., 1994; Watt, Pyle, & Mather, 2009). Numerous case studies exist which have documented earthquakes followed by heightened volcanic activity (Linde et al., 1994). In addition to this, numerical models have been run in order to determine how earthquakes might trigger heightened volcanic activity (Hill et al., 2002; Namiki & Manga, 2006; Ichihara & Brodsky, 2006). However, very little research has been carried out on the physical effects of seismic waves interacting with magma chambers (Bagdassarov, 1994; Walter et al., 2007). Existing literature suggests theoretical reasons for why earthquakes trigger eruptions; however this has been poorly constrained. The purpose of this project is to examine the effects of seismic shaking on the behaviour of bubbles within magma. Bubbles drive volcanic eruptions (Namiki et al., 2016; Llewellin & Manga, 2005; Namiki & Manga, 2006) and their behaviour during shaking may give us insight into how volcanoes are triggered by earthquakes. Through the data gathered from these experiments it is hoped a better understanding may be gained on how seismic waves may affect bubbles within a volcanic magma reservoir or conduit.

2.1 Project Aims

My overall research question is to assess how bubble behaviour is affected by shaking in viscoelastic fluids as an analogue for bubbly magma. The experimental process was set up in order to answer these questions;

- By shaking bubbles in viscoelastic fluids how is bubble rise rate and shape affected?
- What effect do system parameters have on bubble behaviour during shaking?
  - Viscosity (Pa s)
  - Bubble size (m)
- What effect do shaking parameters have on bubble behaviour?
  - Displacement (mm) and frequency of shaking (Hz)
  - Acceleration of shaking (g) as a function of displacement and frequency where $g = 9.81$ m s^{-2} (Bueche, 1970).
  - Duration of shaking (seconds)
- What is the physical mechanism for accelerated rate of rise of a bubble during shaking?
- What are the implications of bubble behaviour during shaking for natural geological systems?

2.3 Thesis layout

A comprehensive literature review has been carried out on subjects pertaining to this project. In particular, literature on volcanic activity triggered by earthquakes, volcanic process related to this project, and past research and experiments which informed experimental processes for this project. The methodology and equipment used in the experiments and how they have been analysed have then been outlined, with information on equipment, materials, variables and their limitations where necessary. The results from the experiments carried out are then presented. In the following discussion results are presented critically to answer the aims set out for the project, particularly with regards to their implications for bubble migration within both closed and open volcanic systems. These results have then been modelled numerically to determine if advective overpressure changes can be connected to the results from the experiments. Finally, the limitations and areas of further study have been laid out and my overall conclusions presented.

3. Literature Review

3.1 Introduction

Statistical analysis has estimated that 0.4% of volcanic eruptions have been triggered by an earthquake within days of the initial activity (Bebbington & Marzocchi, 2011). Earthquakes trigger both volcanic unrest and eruptions, and have been the subject of numerous studies over the past century (e.g. Manga & Brodsky, 2006; Linde & Sacks, 1998; Linde et al., 1994; Eggert & Walter, 2009). These studies aim to verify the phenomena (e.g. Eggert & Walter, 2009; Hill et al., 2002; Marzocchi, 2002) and to investigate possible physical triggering mechanisms (Namiki et al., 2016). Anecdotal (Troll et al., 2015) and statistical evidence (Hill et al., 2002) exists in abundance and supports the supposition that seismic activity can and does trigger volcanic activity (e.g. Bonali et al., 2012; Walter et al., 2007; Namiki et al., 2015; Manga & Brodsky, 2006; Ichihara & Brodsky, 2006). Evidence suggests that this phenomena can occur in both the near and far field (Manga & Brodsky, 2006) and over a wide temporal range, from seconds to years (Eggert & Walter, 2009). It has occurred across the spectrum of volcano types, with no clear differentiation due to composition or morphology (e.g. Barrientos, 1994; Eggert & Walter, 2009; Linde & Sacks, 1998; Manga & Brodsky, 2006; Marzocchi, Scandone & Mulargia, 1993; Ukawa, 2005).

One of the most widely cited cases for earthquake triggered eruptions is the 1960 eruption of Puyehue-Cordón Caulle. The volcano erupted approximately two days after the Mw 9.5 Valdivia earthquake in Chile, 240 kilometres away (Linde & Sacks, 1998; Bonali et al., 2012; Eggert & Walter, 2009; Barrientos, 1994). Eruptions from Hawaiian volcanoes are often associated with Mw 6+ seismic activity at distances of approximately 20-30 kilometres away (Eggert & Walter, 2009; Walter & Amelung, 2006). Similarly, Mt Vesuvius has been connected with volcano-tectonism correlations (Marzocchi et al., 1993). Additionally, volcano seismicity was influenced at Long Valley Caldera following the 1992 Landers earthquake, leading to changes in geothermal activity (Linde & Sacks, 1998). Volcanoes on Iwo Jima in Japan showed heightened activity following seismic activity at distances of 200 kilometres away (Ukawa, 2005; Eggert & Walter, 2009). Perturbations were recorded following the 2002 Denali Mw 7.9 earthquake at distances of up to 3,660 kilometres away in California and Yellowstone National Park (Manga & Brodsky, 2006).

Triggered activity includes eruptions as well as other signs of unrest at the volcano and at geothermal systems associated with them (Crews & Cooper, 2014; Jousset et al., 2013; Carbone et al., 2009). Degassing of volcanic systems has been noted after earthquakes in open systems (Jousset et al., 2013) and gravity surveys have shown mass relocation under volcanoes (Carbone et al., 2009). Mass relocation is presumed to be due to bubble or crystal matter relocation. Degassing events are of equal interest to eruptions for this project as the experiments aim to look at bubble behaviour and outgassing may indicate bubble migration. There are also several instances of mud volcanoes becoming active following earthquakes (Davies et al., 2008).

3.2 Eruptive processes with regards to volatiles and bubbles in magma

Bubbles are integral to behaviour in volcanic systems (Heap et al., 2015; Namiki et al., 2016; Namiki & Manga, 2005; Beckett et al., 2014). Nucleation and growth of bubbles from the volatiles dissolved within magmas are a complex and important control on volcanic behaviour (L'Heureux, 2009; Sigurdsson, 2000). All magmas typically contain amounts of H_2O, CO_2, sulphur species, and Cl, in order of most abundant to the least (De Vivo et al., 2005; Naumov et al., 2010). Studies of melt inclusions have shown that volatile composition within different magmas can be highly varied, depending on the magmatic source and tectonic setting and history (Naumov et al., 2010; Sigurdsson, 2000). The presence and amount of volatiles affects crystallization, melting temperature, density, and the viscosity of magma, which in turn affect the eruptive behaviour of the volcano (e.g. Huppert & Woods, 2002; Mcintosh et al., 2014; Baker et al., 2005). Of these volatiles H_2O is the most dominant and is often considered the most important with regards to volcanic characteristics and behaviours (Baker et al., 2005; Sigurdsson, 2000).

To understand the effects of seismic activity on magma it is important to understand the role of volatiles in volcanic systems (De Vivo et al., 2005; Gurenko et al., 2005; Baker et al., 2005). Magma contains volatiles dissolved into the melt (Divoux et al., 2011). Decompression of the magma occurs by upwards magma movement or reduction in magmastatic or lithostatic pressure, causes volatiles to become supersaturated. Exsolution and bubble formation occurs when the melt reaches a critical oversaturation of volatiles (L'Heureux 2009; Taddeucci et al. 2006), a value which is controlled by pressure or depth exerted on the magma (Huppert & Woods, 2002). As volatiles form bubbles, they undergo a large increase in molar volume increasing the buoyancy of the magma through density

differences (De Vivo et al., 2005). These changes increase the pressure in the magma chamber through expansion and can result in upward transport of the magma to the surface. Volatiles influence the eruption style, size, and timing (Huppert & Woods, 2002; Sigurdsson, 2000).

The volume of bubbles, both overall and on a singular basis, nucleated within magma is highly complex and dependent on numerous factors (Sigurdsson, 2000). These include volatile concentration available in the given magma, mobility and diffusion of constituents within the magma, pressure and temperature, and viscosity (Dingwell, 2006; Baker et al., 2005; L'Heureux, 2009). The velocity at which a singular bubble will rise is controlled by the volume of the bubble, the viscosity of the fluid (Talaia, 2007; Baz-Rodríguez et al., 2012). The ratio of melt to crystal matter in the magma will also affect how bubbles move by introducing impediments to rise (Sigurdsson, 2000; Parmigiani et al., 2016). These will contribute to how the bubbles may affect pressure in the conduit through rise (Lejeune et al., 1999; Dingwell, 2006). In more viscous magmas, such as rhyolites, bubble growth may be limited by the ability of bubbles ability to diffuse and coalesce. In less viscous magmas the ability of bubbles to move through the fluid and coalesce can lead to larger bubbles, which then increase in upwards rise velocity (Baz-Rodríguez et al., 2012). However, there is no definitive rule for bubble size variation in different magma compositions. Bubble size may range from microns in size up to gas slugs which may be meters in diameter (Del Bello et al., 2012; Sigurdsson, 2000). Bubble and magma rise is buoyancy controlled, and in high viscosity systems the rise of the bubbles may be coupled with the rise of magma (Gualda & Anderson, 2007), whereas in low viscosity systems bubbles may rise more independently than the magma (De Vivo et al., 2005). In both scenarios pressure can increase to levels that can potentially trigger volcanic eruptions.

Bubble behaviour and bubble deformation, or shear, is a product of its capillary number (Rust et al., 2003; Roman & Cashman, 2006). This may be through pure or simple shear (Rust et al., 2003). The capillary number represents the ratio of the surface tension of the fluid to the forces of viscosity attempting to shear it. If the surface tension is overcome by the force of the viscosity or by shear strain rates acting upon it the bubble is deformed. The amount to which bubbles are sheared, losing their spherical shape, can affect how the two-phase magma behaves as a whole (Rust et al. 2003). Behaviour of the bubble on its own will also be affected by its morphology, causing changes to bubble rise rate as the frictional surface changes (Baz-Rodríguez et al., 2012; Parmigiani et al., 2016; Lejeune et al., 1999).

3.3 Non-seismic triggering of eruptions

Bubble nucleation, growth, and movement is the main driver behind magmatic volcanic activity (Pyle & Pyle, 1995; Hill et al., 2002; Linde et al., 1994; Mcintosh et al., 2014). To understand how earthquakes may trigger volcanic activity it is important to first understand how magmatic activity is triggered. Volcanic systems are stochastic and highly complex, which makes the understanding of the triggers of increased activity difficult (Pyle & Pyle, 1995).

The process of bubbles exsolving, expanding, and migrating can lead to a magmatic eruption of a volcano if it causes a pressure increase great enough to overcome overburden pressure, cracking and unsealing the system (De Vivo et al., 2005; Pyle & Pyle, 1995; Mcintosh et al., 2014). There are three main ways in which volatile bubbles can be nucleated, expanded, and begin migrating in a sealed magmatic system leading to magmatic activity (Pyle & Pyle, 1995). It can be initiated by (1) intrusion of magma of a difference temperature or composition changing the solubility of the volatile with in the mama (Huppert & Woods, 2002; Pyle & Pyle, 1995), (2) anhydrous crystallization in the magma leading to a second boiling bubble exsolution phase (Pyle & Pyle, 1995), and (3) bubbles rising and causing advective overpressure in the closed magmatic system (Pyle & Pyle, 1995; Steinberg et al., 1989). Various mechanisms exist for initiating volcanic activity, but, as this project deals with bubble migration through seismic activity only these triggers have been focused on.

The growth of bubbles in a melt which is enclosed in a system must overcome the confining pressure necessary to initiate an eruption. Pyle and Pyle (1995) discuss the failure criteria used to determine whether the pressure envelope will be exceeded. For a melt enclosed in an elastic medium the maximum fractional volume change of the body before failure is;

$$\Delta V_c/V \text{-} 2\sigma/y \text{ (Pyle \& Pyle, 1995)}$$

in which σ is the tensile strength *[(2-8)x10^6 Pa]*, and y is country rock rigidity ($\sim 10^{10}$ Pa) (Pyle & Pyle, 1995). Therefore, for a sealed system magma chamber in which $\Delta V_c/V < 10^{-3}$ bubble volume introduced exceeding ~0.1% of the total volume of the system will cause failure and eruption of the previously sealed magma (Tait et al., 1989). Similar calculation have been made around an individual bubble (Zhan et al., 1997) and experimentally measured within a bubbly melt (Spieler et al., 2004)

3.4 Seismic shaking

A diverse range of earthquake magnitudes have been associated with triggering volcanic activity (e.g. Manga & Brodsky, 2006; Sánchez & McNutt, 2004; Villalobos, 2011) and research has shown that both near- and far-field source events have been implicated in triggering (Walter, 2007). Peak ground acceleration (PGA) or acceleration, is a function of amplitude (x) and frequency (f); $a = -(2\pi f)^2 x$. Seismic shaking, for the purpose of this project, will be considered as acceleration, or peak ground acceleration (PGA).

The 1992 Landers earthquake triggered activity up to 1,200 kilometres away from the source, both seismic and at geothermal fields (Hill et al., 2002). This earthquake produced high PGAs, up to 0.97 g near the source (Cramer & Darragh, 1994). Two days after the 2011 Mw 9.0 Tohoku-oki earthquake the volcano Shinmoedake, located 1,300 kilometres away on Honshu Island, showed heightened activity (Wang et al., 2011). Shinmoedake had been active previously that year but was quiescent before the earthquake, leading to the assumption that the increased activity was seismically triggered. The Tohoku-oki earthquake produced some of the highest PGAs recorded, up to 2.7 g (Kurahashi & Irikura, 2011).

The 1960 Mw 9.5 Valdivia earthquake triggered activity at Puyhue-Cordon Caulle (PCC). Weischet (1963) reported PGA of 0.25 – 0.3 g based on the Mercalli intensity X. However, these PGAs are likely highly inaccurate and the PGA produced was likely much greater (Villalobos, 2011). Work by USGS estimated that shaking at PCC was strong to very strong, with a peak acceleration of 12-22 g (USGS, 2016). This situation illustrates the difficulties in determining PGA at volcanos produced by the triggering earthquakes. In many cases no acceleration data is available for the volcanoes, particularly for older eruptions. Modern monitoring at volcanic centres often includes seismic monitoring (Linde & Sacks, 1998), which should be of immense interest to this field.

Shaking produced by an earthquake may last from seconds to minutes long (Trifunac & Brady, 1975). The longest recorded earthquake, the 2004 Sumatran-Andaman Mw 9.3 lasted just under 10 minutes (Sørensen et al., 2007). Five months later the previously quiescent Barren Island Volcano erupted. This activity is considered to be linked to the Sumatran-Andaman earthquake (Sheth, 2014).

3.5 Statistical analysis

Numerous statistical analysis studies have been carried out to demonstrate the correlation between earthquake and heightened volcanic activity (Hill et al., 2002; Linde & Sacks, 1998; Marzocchi et al., 1993; Marzocchi, 2002; Eggert & Walter, 2009). Conclusions from these statistical studies confirm that there is a positive temporal correlation between earthquakes and volcanic activity; 0.4% of volcanic activity was triggered by tectonic activity within days of the earthquake (Manga & Brodsky, 2006). A number of applicable studies have used statistics to look at the temporal and spatial relationship between earthquake and increases in volcanic activity (Bonali et al., 2012). However, the information used in each of these studies vary widely due to incomplete data sets, low numbers of events, and instances of coincidence (Bebbington & Marzocchi, 2011). However, their overall results indicate that a positive correlation exists.

The tectonic setting of Mt. Vesuvius is closely related to the Southern Apennines mountains, a NE-SW trending active fault system (Marzocchi et al., 1993). Interaction of this fault system and Mt. Vesuvius has been investigated by running a detailed statistical analysis of the activity of both. The Southern Apennines and Mt. Vesuvius were chosen as they both have relatively long and reliable records available. Using these records they looked for correlations between the periods of seismic activity in different tectonic blocks and eruptions at Mt. Vesuvius within the same time window. They found a positive correlation between seismic activity from some tectonic blocks and eruptions at Mt. Vesuvius. However, they state that the triggering mechanism for this is unclear.

Marzocchi (2002) continued work in this field by identifying non-random patterns in volcanic eruptions following great tectonic earthquakes (Marzocchi, 2002). Instead of focusing on one tectonic region, as with the previous study of Mt Vesuvius, the study looked globally. Using records from the Smithsonian Institute, eight VEI 5+ events from the last century were chosen. These were then compared to seismic records. Marzocchi's analysis found that there was significantly correlation between earthquakes and eruptions which occurred 0-5 years and 30-35 years previous. These occurred at distances up to 1000 kilometres away.

The 1992 Mw 7.3 Landers earthquake in Southern California triggered seismicity at distances of up to 1000 kilometres away. Activity induced included geothermal and seismic activity at the Long Valley Caldera approximately 550 kilometres away (Linde & Sacks, 1998). The idea that seismicity could be dynamically triggered in a volcanic system over such a distance

prompted a statistical study by Linde and Sacks (1998) looked specifically at far-field triggering. Similar to the work by Marzocchi (2002) they looked at global historical records of eruptions and earthquakes. However, their temporal range was limited to only two days, instead of up to 35 years after the earthquake. They compared the reports of increased volcanism with earthquake activity at different spatial ranges. It was found that one to two days following a significant earthquake (magnitude 7+) volcanism statistically increased within a 750 kilometre range.

Manga and Brodsky (2006) carried on with the work presented by Linde (1994) and Linde & Sacks (1998) with several variations. They considered volcanic eruptions occurring within five days of large earthquakes, within an 800 kilometre radius (Manga & Brodsky, 2006). Only volcanic eruptions of ≥ VEI 2 were considered. Like the work of Linde and Sacks (1998) they found that volcanic activity increased following large earthquakes. Statistically 0.4% of volcanic eruptions followed with five days of large earthquakes, both near and far field. While this does not seem high it is statistically significant.

Recent work by Eggert and Walter gives a comprehensive overview of potentially triggered events and reviews statistical analyses previously carried out (Eggert & Walter, 2009). They present their own findings on a sub-regional volcanic scale and several temporal ranges. The data sets used are similar to that of Marzocchi (2002). However, they have used only data from 1990 onwards. The data sets from before 1990 tend to be less complete and less accurate due to inferior monitoring equipment and unreliable global coverage. One of the main differences in this study was that the full catalogue of events is employed for the statistical analysis, instead of focusing on specific case studies. They found that a statistical correlation existed and that volcanism was triggered in many different tectonic settings. However, volcanoes located in the Ring of Fire showed the highest correlation coefficient. Triggering was also shown to occur over large temporal and spatial ranges. They also point out that triggering is most evident in the near-field and most triggered activity occurs on the same day as the seismic event.

South America has been the focus of numerous studies due to its tectonic setting (Dzierma et al., 2012; Watt et al., 2009; Walter, 2007). The presence of a subduction zone capable of producing Mw 7+ earthquakes and a relatively large number of active volcanoes make it highly suitable for volcano-tectonic studies (Watt et al., 2009). Watt et al. (2009) examined the background volcanic activity and compared levels before and after large earthquakes.

They found that background levels increased for approximately 12 months following Mw 8+ events. This was most notable in 1906 and 1960, following several large earthquakes. The location of potentially induced volcanic activity was up to 500 kilometres.

A study by Bonali et al. (2012) focuses on a large catalogue of earthquake and volcanic events from the Southern Volcanic Zone (SVZ) in the South American Andes. The temporal range used is from 1906 to present. This study looks at statistical analysis and also focuses on static stress changes as a possible trigger for volcanic activity. Using previous work by Delle Donne et al. (2010) they determine a radius in which volcanoes may be statically triggered into activity by Mw ≥8 earthquakes in the SVZ region. This was worked out by relating the earthquake magnitude (M), to the distance (R) giving an empirical maximum distance for possible volcanic activity. Then using a database of relevant volcanic activity they examined volcanic activity within that radius within five years. In order to assess triggering mechanisms they also correlate the depth of magma chambers, magma composition and rheology, the tectonic setting and dimensions of the volcanic edifice. By pinpointing the volcanic feeder systems and their nature they could better examine the stress changes. They propose that the change in static stress from the earthquake may cause an "unclamping" of diking structures, allowing increased activity. This was achieved through numerical modelling of the static induced stress changes on conduits at affected volcanoes. They conclude that Mw ≥8 earthquakes can cause static stress changes in volcanic systems, causing an unclamping of feeder systems, which can occur at distances up to 353 kilometres away, resulting in possible increased activity. Magma chamber depth, silica content and geometry of the system also appear to be influencing factors on whether a volcanic system will be triggered into activity (Bonali et al., 2012). Shallower magma chambers appear to be more affected and systems with higher silica content were more likely to experience "awakening".

Hydrothermal activity and mud volcano eruptions also occur in response to earthquakes (Manga et al., 2009; Davies et al., 2008). A study by Manga et al. (2009) compiled observations of mud volcanoes and similar geologic systems (liquefaction, groundwater, faults, and geysers) showing aberrational activity after an earthquake. They found that there was a magnitude-distance threshold for triggering these events. It was also found that volcanic, geothermal, and mud volcanic systems which were already active were more susceptible to increased activity than systems which had been previously dormant.

Several studies have discussed heightened geothermal activity in the Long Valley Caldera, California (Sánchez & McNutt, 2004; Manga et al., 2009; Linde & Sacks, 1998). Following the 1992 Landers earthquake heightened activity was noted and is attributed to far field triggering. The effects of seismic waves on geothermal systems have also been noted during geothermal tomography studies which use seismic (Jousset et al., 2015).

Statistical analysis has shown that volcanic activity can be induced by earthquakes. It occurs in a range of settings and over large spatial and temporal ranges. However, the physical mechanism brought about by the seismicity which triggers the eruption is currently poorly understood. However, there exist several studies which use numerical modelling to investigate possible triggering mechanisms.

3.6 Numerical modelling

Numerical modelling has been carried out in numerous studies to test physical models against possible physical mechanisms for triggering heightened volcanic activity following an earthquake (Walter, 2007; Bonali et al., 2012; Bebbington & Marzocchi, 2011; Ichihara & Brodsky, 2006). Earthquakes triggering further seismic activity due to crustal stress changes have been extensively studied (King et al., 1994). The rupture of a fault can lead to Coulomb stress changes being placed onto surrounding faults and lead to subsequent failure (King et al., 1994). This process has been extensively modelled and the same method has been applied to volcanic systems to determine if a static stress change may have increased pressure on a magmatic system (e.g. Bonali et al., 2012; Fujita et al., 2013; Gudmundsson & Andrew, 2007; Walter et al., 2007). If the static change is large enough to cause a significant pressure change then volcanic activity may be triggered.

Bonali et al. (2012) has explored numerical models of clamping and unclamping of magmatic pathways. This was carried out by computing the normal static stress changes following the earthquakes. These were found to have likely triggered new or heightened volcanic activity. Stress changes were resolved on magma conduits and examined for clamping or unclamping changes, from weak to high. They found that new activity occurred in areas which experienced weak clamping while awakening events (i.e. volcanic activity from a quiescent volcano) tended to coincide with high unclamping events. Larger earthquakes were associated with higher numbers of possible unclamping events and the models indicate that magma conduit unclamping occurs more strongly at closer distances to the seismic event.

They suggest that the unclamping of the system may lead to dike intrusions, magmatic movement, and subsequent eruption.

A similar numerical study was carried out on two volcanoes in Kamchatka, Karymsky Stratovolcano and the Akademia Nauk Caldera (Walter, 2007). The volcanoes are part of the same NE-SW trending fault complex. Both volcanoes erupted two days after a Mw 7.1 located 10-20 kilometres away. Karymsky volcano has been very well monitored and is active; however the Akademia Nauk Caldera was considered dormant and was apparently awakened by this event. The area is well monitored and geodetic measurements from this period were available. Using Poly3D coding 3-dimensional models were built to examine the stress changes in the fissures at both volcanoes. They found that inflation of the magma chamber prior to the earthquake may have raised the Coulomb failure stress leading to the earthquake. The static changes caused by this likely then lead to an unclamping of the north-south magmatic fissure leading to eruption at both volcanoes. They also hypothesize in the paper that dynamic triggering may have also had some influence on the triggering.

3.7 Mechanisms for triggering of volcanic activity following seismic activity

The triggering of volcanic activity due to earthquakes can occur through static triggering, dynamic triggering, or a combination of both (Walter, 2007; Walter et al., 2007; Watt et al., 2009; Bonali et al., 2012). Static triggering occurs when tectonic movement induces a crustal stress change that can affect the volcanic system (Walter et al., 2007; Linde & Sacks, 1998; Hill et al., 2002; Bebbington & Marzocchi, 2011). This was briefly described in the previous section. Resulting activity may not change for days to years depending on the state of the system at the time of the event. Dynamic triggering occurs due to the transient stress changes, caused by the passing of the seismic waves themselves (Walter et al., 2007) inducing changes in volcanic system. These changes may have carry on effects that trigger activity either immediately or sometime after event.

The mechanisms which are thought to trigger activity due to static triggering have been briefly discussed in the numerical models section. Static, or Coulomb, stress changes, (King et al., 1994), in the volcanic edifice can cause a clamping or an unclamping of conduits. This can then cause a pressure change within the system (Manga & Brodsky, 2006; Fujita et al., 2013). Pressure shifts may lead to overpressure or a decrease of overpressure leading to

exsolution of magmatic volatiles. Exsolution of volatiles due to pressure changes in the system may then result in triggered activity.

On May 22, 1960 the largest recorded earthquake, a Mw 9.5, occurred in Chile, off the coast of Valdivia (Hill et al., 2002; Walter & Amelung, 2007; Dzierma et al., 2012; Watt et al., 2009). Thirty-eight hours later Puyehue Cordón-Caulle erupted 240 kilometers away, its first eruption in sixteen years (Watt et al., 2009; Lara et al., 2004; Fujita et al., 2013). In the three years following the earthquake three more volcanoes erupted, as far away as 500 kilometres (Fujita et al., 2013). It has been postulated that static changes caused an unclamping of the magmatic system leading to the fissure fed eruption (Watt et al., 2009; Bonali et al., 2012; Walter & Amelung, 2007). Unfortunately, very little is known about the state of the volcanic system at that time as there was very little monitoring existed in the area around Puyehue Cordón-Caulle.

Dynamic triggering is caused by the transient passing of seismic waves (Walter et al., 2007; Crews & Cooper, 2014). Dynamic stresses decay more gradually then static stresses over distance, which accounts for why dynamic triggering may occur over further distances than static (Manga & Brodsky, 2006). The effect of how this may affect magmatic systems is still not well understood. However several mechanisms have been postulated. This dynamic stress change could cause bubbles to nucleate, more gas to diffuse into bubbles, or bubbles to be dislodged from the crystals or crystal mush zones to collapse (Boudreau, 2016). In turn these processes may drive convection or overturn of a magma body. Pressure may increase by advective overpressure as bubbles rise. These could lead to advancing the clock of a volcanic system and result in seismically induced activity in the magmatic system (Pyle & Pyle, 1995).

3.7.1 Nucleation

A study by Crews & Cooper (2014) found that Rayleigh and P seismic waves can cause CO_2 bubble nucleation and migration through dilation strain in water. This study was in response to co-seismic borehole water level rise during the 1992 Landers, California Mw 7.3 earthquake. As the water level rise could not be explained through static stress changes (Roeloffs, 1998) it was proposed that dynamic stresses triggered the nucleation and growth of bubbles in CO_2 rich water (Crews & Cooper, 2014). They propose that this may occur when dilation seismic wave propagation causes the fluid pore pressure in the groundwater system to drop below the pressure in the existing bubbles. Once the propagation waves have passed

the pressure changes cause the CO_2 bubbles to compress and the groundwater in the pores is displaced upwards.

3.7.2 Rectified diffusion

Rectified diffusion may affect bubble growth during transient seismic waves through mass transport (Manga & Brodsky, 2006; Ilinskii et al., 2008; Ichihara & Brodsky, 2006). Seismic waves cause bubbles to oscillate according to the amplitude of the waves, resulting in expansion and contraction (Ichihara & Brodsky, 2006). When contracting, volatiles will diffuse back into the under-saturated melt and then diffuse back into the bubble during expansion. When contracted, the surface area of a bubble is smaller than when expanded meaning that the rate of diffusion of volatiles back into the melt during seismic waves will be lower than the rate diffusing into the bubble. Thus, the net gain of volatiles into the bubble will be greater than that which is gained by the melt. Bubble size may be increased through this process and lead to heighten pressure within the system.

Rectified diffusion has been considered through modelling to determine whether it was a viable triggering mechanism (Ichihara & Brodsky, 2006). Results of the numerical models suggested that significant pressure changes in the system only occurred when the magma was sufficiently oversaturated with volatiles before interacting with seismic waves (Manga & Brodsky, 2006). While it may have a small contribution to triggering it is not considered a strong contributor to increased activity following seismicity.

3.7.3 Advective overpressure

Advective overpressure is the process by which pressure increases in a closed system due to the ascent of bubbles within that system (Manga & Brodsky, 2006; Linde et al., 1994; Pyle & Pyle, 1995; Sahagian & Proussevitch, 1992). This makes it of particular note for this project as bubble rise rate affects pressure increases. This mechanism has been proposed as a trigger for activity in geothermal and volcanic systems over very large distances (Linde et al., 1994; Steinberg et al., 1989; Pyle & Pyle, 1995; Sahagian & Proussevitch, 1992) due to bubbles being shaken loose by transient seismic waves. It has also been suggested that this is not a stand-alone process and could work in concert with magma chamber convection, overturn, or other processes (Manga & Brodsky, 2006).

There have been several papers which look at advective overpressure from a numerical and experimental basis (Pyle & Pyle, 1995; Sahagian & Proussevitch, 1992; Sahagian, 1993; Bagdassarov, 1994). Results of these may be modelled and applied to magmatic systems to see if pressure changes significantly. Advective overpressure was tested experimentally using balloons rising in sealed chambers filled with an incompressible fluid (Sahagian & Proussevitch, 1992) and then applied mathematically to magmatic systems (Linde et al. 1994). The first experiments (Sahagian & Proussevitch, 1992) placed a bubble into the bottom of a cylinder which was filled with a fluid and sealed completely. Temperature and volume remain constant in the system throughout and the pressure increase is based on an existing bubble, nucleation is not taken into account.

The system, when the bubble is at the base of the cylinder has an initial pressure of P_0. The pressure at the top of the system is $P_0-\rho gh$, where ρ is the density of the fluid, g is acceleration due to gravity, and h is the height which the bubble ascends. The bubble rises through the system, with no diffusive action taking place with the surrounding fluid. Once the bubble has risen to h, the pressure at the top of the system must now be P_0, and the pressure at the bottom is therefore $P_0+\rho gh$, and pressure in the system has been raised by ρgh. This formula does not take into account bubble growth, or the increase of pressure within the bubble in an incompressible fluid due to decreased overburden pressure as the bubble travels upwards (Pyle & Pyle, 1995). This formulaic relationship is of great interest to the experimental part of this project. If bubbles are found to rise faster during shaking then the distance travelled, h, will have increased. This will result in a higher final pressure within the system.

The speed of the bubble rise and therefore the size and overall volume of bubbles in the system affect advective overpressure. These parameters control the extent to which advective overpressure can increase the pressure of the system (Furbish, 1997). A smaller bubble would have little effect on the overall pressure of a system but many small bubbles or larger bubbles, giving a greater overall volume of gas rising in the system, will cause a greater increase. However, it is difficult to determine the volume of a magma chamber and the volume of bubbles within. The application and efficacy of advective overpressure as a trigger has been debated (Bagdassarov, 1994; Pyle & Pyle, 1995).

3.7.4 Magma chamber convection

Passing seismic waves may affect loosely bound crystal mush in magma chambers, causing them to sink within the chamber (Hill et al., 2002; Manga & Brodsky, 2006; Namiki et al., 2016; Plesset & Prosperetti, 1977). The sinking mass of crystal mush is replaced by magma from further down within the chamber through convective forces. This may also detach previously nucleated bubbles or form migration paths for them (Boudreau, 2016; Parmigiani et al., 2016). If the rising magma is destabilized enough due to pressure changes then exsolution of volatiles may occur. Vesiculation of this rising magma can conceivably lead to a pressure increase resulting in eruption. Work by Manga and Brodsky (2006) concluded that this may be a viable trigger if the dynamic stresses are high enough to release crystal masses. However, they note that the state of a magma chamber must be under very specific conditions for this to occur (Manga & Brodsky, 2006). This process, as previously indicated, may also work together with advective overpressure. Convection leading to bubbles rising will then lead to increased pressure through the bubble advection, without taking exsolution and bubble growth into account (Pyle & Pyle, 1995).

3.7.5 Bubble Cavitation

While many believe that bubble cavitation is a less likely trigger for volcanic activity it has been suggested as a possible contributor for increased pressure in systems (Plesset & Prosperetti, 1977; Kedrinskii et al., 2005; Kedrinskii, 2008). Bubble formation and collapse, or cavitation, can occur during agitation of a fluid. Cavitation is the process by which bubbles form and collapse, resulting in the formation micro-jet of intense pressure (Plesset & Prosperetti, 1977). This pressurized jet released upon collapse of bubbles has been proposed as a mechanism for increased pressure in a sealed magmatic system (Blake & Gibson, 1987). This process has been extensively studied with regards to fluid and bubble dynamics in industrial systems and on propellers (Blake & Gibson, 1987; Plesset & Prosperetti, 1977; Crews & Cooper, 2014). It is important processes for analysing industrial equipment as the micro-jets produce enough pressure to degrade metals. However, little work, modelling or experimental, has been done on the application of this process to magma chambers and the likelihood of cavitation occurring in magma chambers during shaking (Ichihara & Brodsky, 2006).

3.8 Previous work used to inform experimental set up of this project

Very little experimental work had been carried out on the effects of shaking, or forced oscillations, on bubbles within viscoelastic fluids. Therefore the previous experimental work used to inform the basis of the experiments of this project comes from a range of fields. They include non-shaking volcanology experiments and fluid dynamics. However, there have been previous shaking experiments which have looked into different aspects of fluid and bubble behaviour during forced oscillations (Namiki et al., 2016; Llewellin et al., 2016). Previous analogue experiments have been used in order to determine the physical and rheological properties of the fluid to be used for the experiments. Several studies which with magma rheology and its physical properties and have been used to determine the materials used in the experiments for this project.

3.8.1 Bubble analogue experiments

While few experiments have been carried out on shaking of volcanic systems there are still several which are applicable. Large earthquakes have been known to induce sloshing in water and petroleum tanks, resulting in damage to the tank (Housener, 1963; Housner, 1957). Experimental magma sloshing investigated whether earthquakes may cause sloshing, or the oscillatory movement of fluids in confinement (Namiki et al., 2016). Analogue experiments were designed and simulated earthquake induced sloshing in magma chambers, to see how this might affect a volcanic system. They concluded that the sloshing of the magma could increase the mobility of the volatiles in the melt and possibly collapse foams in the magma.

The experiments carried out by Namiki et al. (2015) used partially and fully filled 0.24 x 0.24 x 0.9 m rectangular tank. These conditions mimic both sealed magma chambers, and open reservoirs, such as conduits or lava lakes. The fluids in the tank were density stratified, with a foam layer overlying the liquid layer. The fluid used as a magma analogue was glucose syrup with viscosities from 0.1 Pa s to 90.0 Pa s. The viscosities used were chosen to mimic a basaltic melt with a sub-solidus and low crystal fractionation, which are reported to have a range of 1 - 10^4 Pa s viscosity. Surface tension of the fluid was similar to that of a silicate melt, 0.01-0.1 N m^{-1}. Bubbles were then added as the top layer by reacting sodium bicarbonate with citric acid. Volume of the bubbles added was controlled using the amount of reactants. Plastic particles were added to the solution to mimic crystals within the melt and

provide possible nucleation points for bubbles. In the experiments the following was varied; fluid viscosity, bubble volume, fluid layer height, and shaking parameters.

The tank was attached to a GeoSIG GSK-166 shake table. The shaking parameters varied the duration of shaking, displacement (*D)*, and frequency (*f*). These variations, combined with the fluid variations result in 1167 different experimental parameters. The shaking parameters tested up to accelerations of < 1*g*, where $g = 9.8$ m s^{-2}.

These experiments found that when conditions in the tank included vacant space or fluid density heterogeneities shaking induced oscillations of the fluids. When a foam layer was included in the experiment the oscillations, or swaying, of the fluid during shaking caused bubble deformation, rupture and foam collapse. They concluded that magma reservoir geometry, magma density, viscosity, and bubble size and volume were important controls on whether magma sloshing could be induced. The larger the reservoir, the more pronounced and severe sloshing may become. Shaking with a frequency of <1 Hz was found to be unlikely to induce sloshing within realistically scaled reservoir sizes. Frequencies of ~1 Hz affected fluids analogous to low viscosity basalts (< 10^{-3} Pa s), causing foam collapse where bubbles were ~1 mm. Resonance frequency of the materials, if similar to the frequency of the shaking, resulted in greater sloshing effects. Density stratified fluids were also susceptible to sloshing, even in a filled and sealed tank. Their findings suggest that low frequency seismic waves, which are typical of large earthquakes, may cause oscillation of magma in large reservoirs (Namiki et al., 2016).

Work by Namiki et al. (2015) was based on modelling and experimental work looking at the effects of sloshing on fluids in holding tanks (Housener, 1963; Housner, 1957). During earthquakes it was found that water and oil reservoirs and dams could be damaged due to sloshing effects. These effects are examined using evidence from field observations and modelling of fluid dynamics in rectangular reservoirs containing water. For comparison to other fluids discussed, water has a viscosity of viscosity of ~10^{-3} Pa s (Le Corvec et al., 2013). It was found that a sealed system, filled with water or completely empty of water behaved as a single structure during shaking and did not induce damage. However, work discussed by Namiki et al. (2015) found that sloshing did occur in a sealed, filled tank if fluids had density stratifications. Partially filled reservoirs behaved as two separate, dynamic structures during shaking, causing damage to the holding tanks (Housener, 1963; Housner, 1957).

Co-seismic borehole ground-water level rise has been recorded in many areas in response to both near- and far-field earthquakes (Crews & Cooper, 2014). Experimental evidence suggests that this occurs due to gas bubble nucleation and bubble growth which is initiated by seismic waves. Experiments were carried out by sealing a length of porous sandstone within a length of tube. The tube was filled with CO_2 saturated water, with the CO_2 varied depending on experimental parameters, with a confining pressure of 2.758 MPaG and placed under a confining stress of 3.447 MPaG. This simulates borehole ground-water conditions in which CO_2 is dissolved into the water. The pressurized tube is then subjected to confining stress oscillations which imitated dynamic stresses generated by earthquakes. Experiments varied duration, displacement, and frequency. While Crews and Cooper (2014) acknowledge that the experimental process is idealized but results indicate that dynamic stresses can cause CO_2 bubbles in water to nucleate and grow. This occurred at all of the amplitude-frequency parameter pairs tested (Crews & Cooper, 2014).

The effects of bubbles on rheology of a Newtonian fluid were explored by Mader et al. (2013). The magma analogue material for this was golden syrup. Viscosity was measured using a Haake RV20 controlled-rate, rotational viscometer with a concentric-cylinder sensor. As viscosity for this fluid is temperature dependant this was kept stable for experiments. Bubbles were introduced into the fluid by way of a Monodomix aerator and injection of nitrogen gas. Once the nitrogen bubbles were added to the fluid the two-phase fluid was poured into a 10 cm x 10 cm x 100 cm tank. The bubbles were left to rise for approximately one week at room temperature, until they formed a stratified rise column. Bubble size distribution was determined by pressing the fluid between two glass plates, 0.5 mm apart. This was photographed with a digital camera at 4x magnification with an affixed scale bar in the photo.

The two-phase solution in the tank was then subject to sinusoidal varied stresses, or forced oscillations. Deformation after the forced oscillations was then observed and recorded. The deformation found in the samples was similarly sinusoidal to the oscillations and the effects were measurable and repeatable. The response of the bubble suspensions, particularly viscosity, was recorded using a Haake RS100 rheometer. Viscosity of the bubbly fluid varied under the forced oscillations depending on the shear it experienced and the gas volume (Llewellin et al. 2016).

3.8.2 Bubble experiments

Multiple studies and experiments have been carried out regarding the behaviour of bubbles as they are an integral part of volcanic systems. Information which is most relevant to the materials, techniques, and methods is used for the experiments in this project. These experiments do not involve shaking but do include bubbles within viscous and viscoelastic fluids.

Studies which have examined the effects of decompression on bubbles within viscoelastic fluids (e.g. Namiki & Manga, 2006; Namiki & Manga, 2005; Taddeucci et al., 2006). Namiki and Manga (2006) conducted a series of experiments using viscoelastic fluids in vertical shock tubes in order to look at the effect which decompression may have bubbly magmas (Namiki & Manga, 2006; Namiki & Manga, 2005). In these experiments a bubbly fluid, water mixed with xanthan gum, was placed into a shock tube. Bubble stability was maintained by the addition of 0.4% hand soap to the fluid. Viscosity was controlled by the xanthan gum to water ratio. Bubbles were added with a hand mixer. Vesicularity of the fluid was controlled by duration of mixing. Bubble sizes were measured with a microscope prior to decompression and have been assumed to have uniform distribution. The tube was separated from a low-pressure tank by a diaphragm. The pressure difference in the tank was lowered to the point that the diaphragm ruptured a refraction wave propagated through the shock tube. The rapid decompression of the bubbly fluid caused by this was filmed using high-speed cameras. The rate of decompression was controlled by varying the thickness and number of the diaphragms. The rate of decompression and pressure difference, viscosity of fluid, and initial vesicularity of the fluid were varied through the experiments (Namiki et al., 2016).

Results of these experiments found that fluids with higher initial vesicularity, and larger pressure differences resulted in more rapid expansion of the vesicular fluid (Namiki & Manga, 2005). The high-speed camera showed five different types of decompression bubble expansion; fragmentation, partial rupture, detachment, deformation, and no change. When vesicularity of the fluid and the pressure difference were both low little or no change occurred. The rate of decompression affected the shape of bubbles and fragmentation of the bubbly fluid upon decompression (Namiki & Manga, 2006). Fluids which were decompressed more rapidly showed more fragmentation and shear of bubbles. Those which decompressed at a less rapid rate maintained bubble shape and showed volume change and separation.

Similar experiments were carried out by Taddeucci et al. (2006) using viscoelastic fluid in a shock tube to look at the brittle-ductile response to diffusion driven bubble growth (Taddeucci et al., 2006). "Changeable Silly Putty®" was used in the experiments, a viscoelastic silicon polymer, as a magma analogue. Argon gas was dissolved into the fluid under pressure and nucleated into bubbles upon decompression. The fluid had a pressure dependant viscosity from 5×10^4 to 1 x 10^3 Pa s with no apparent effects of the argon gas on viscosity. Viscosity was measured by the rate at which a steel rod sank into the fluid at atmospheric pressure and high pressure (10 MPa). The experiments were controlled in the same manner as the previous shock tube experiments described (Namiki & Manga 2006; Namiki & Manga, 2005). Experiment variables were argon gas saturation, duration, shape and lubrication of the fluid flow path. It was found that the growth and behaviour of bubbles controlled the flow and the fracturing of the fluid during decompression in a manner consistent with observed magmatic processes (Taddeucci et al., 2006).

The acoustic signals produced by gas slugs bursting in vents was experimentally tested (Sánchez et al., 2014). Like the experiments by Taddeucci et al. (2006) analogue experiments were employed. This was carried out by creating bubbles in membrane pressurized chamber and measuring the acoustic signal upon depressurization and bursting of the bubble. Results from this suggest that depths of bursting bubbles within a volcanic conduit may be estimated using their acoustic signal. A similar experiment to this was carried out by Vidal et al. (2010). They investigated the acoustic properties of bubbles bursting at the top of a magmatic conduit using bursting soap bubbles (Vidal et al., 2010). A soap film was emplaced over a cylindrical cavity in a Plexiglas slab. Pressure was increased in the cylinder, causing the bubble to expand until parameters were met at which the bubble burst. Acoustic properties were recorded.

Slow decompression of bubbly fluids, as magmatic analogues, have also been tested (Spina et al. 2016). The experimental process was carried out in the same manner but the materials used are different, and of interest. A silicon oil, similar to that used for the experiments in this project, was used at viscosities ranging from 1 Pa s to 1000 Pa s. Particles were added for some experiments to look at the effects crystal content had on decompression.

3.8.3 Magma analogue materials

A variety of fluids and materials have been used as analogues when modelling volcanic plumbing systems. Since magma is highly complex and spans a large array of physical properties there are a great many parameters which must be taken into account for physical modelling. The material used for analogue experiments is dependent on the processes being modelled and the scale and apparatus of the intended experiments (Merle, 2015).

Magma can span an extremely diverse range of viscosities (Takeuchi, 2015). On the low viscosity end of the scale basalts which are crystal poor, high temperature, and wet can be as low as 10-100 Pa s. Low temperature rhyolites which are crystal rich may be as high as 10^17-18 Pa s (Galland et al., 2015; Holtz et al., 1996). Specific viscosities are dependent of a complex number of factors; temperature, pressure, crystal content, bubble content, overall chemical composition and amount of SiO_2, and applied shear stress and rate (Galland et al., 2015; Kedrinskii et al., 2005; Dingwell & Bagdassarov, 1993). Viscosity dependent on shear rate is particularly important for this project due to its shaking aspects. As they have versatile viscosities silicon oils are most commonly used as an analogue for both low and high viscosity magmas (Galland et al., 2015).

High viscosity magmas have most commonly been simulated using Polydimethylsiloxane (PDMS), a silicon polymer putty (Galland et al., 2015; Klügel et al., 2005; Taddeucci et al., 2006). This is the high viscosity end member of the silicon oils and includes Silly Putty® and similar materials. It behaves as a Newtonian fluid, at typical pressures and temperatures used in modelling experiments (Galland et al., 2015). The viscosity of this fluid can be altered by the addition of other fluids or particles. The addition of particles can also mimic crystal mass within magma, although scaling becomes difficult. The surface morphology of particles is important for altering viscosity as smooth surface may decrease viscosity. Viscosity can also be decreased by the addition of oleic acid.

Silly Putty®, a high viscosity, viscoelastic silicon polymer, has been used to simulate high viscosity magmas (Taddeucci et al., 2006). It is a non-Newtonian fluid; its viscosity is dependent on the rate of deformation (Cross, 2012). Induced stress has a relax time constant of 0.1 s. It's Youngs Modulus for rapid deformation is 1.7×10^{6} N/m². These properties make it useful for low strain experiments or experiments in which viscosity is relatively unimportant.

Low viscosity magmas have been mimicked using fluids from water, silicon oil, honey, golden syrup, cooking oil (Galland et al., 2007), and a wide variety of other fluids (Namiki et al., 2016; Galland et al., 2015). Water is most commonly used, particularly in diking simulations, wherein the water is injected into gelatine moulds (Galland et al., 2015). Water is incompressible, has a density similar to gelatine, a viscosity of ~10^{-3} Pa s and is easily dyed without changing the properties (Le Corvec et al., 2013). Golden syrup has also been used as it has a similar viscosity to some basalts and its transparency make it ideal for interior observation. It has been used in bubble rise experiments (Llewellin & Manga, 2005) and in ignimbrite experiments (Mathieu et al., 2008). Gelatine mixtures have also been used for density driven rise experiments, which have investigated diking and fracturing processes (Rivalta & Dahm, 2006).

3.9 Conclusions

Volcanic activity triggered by earthquakes has been shown to be a possible correlation from anecdotal evidence, statistical evidence, and numerical modelling. Yet there is little experimental evidence of the triggering mechanisms. Experiments have been carried out investigating many aspects of bubble and magma behaviour as well as shaking experiments. However, this literature review has uncovered no experimental or modelling work which examines the effects of shaking on bubble rise rates and the possible effects it may have on magmatic systems.

This project evaluates the effects of seismic shaking on bubble rise rates. Experiments aim to investigate the effects of duration, frequency, displacement, and acceleration of shaking on singular bubbles and look at the effects of viscosity and bubble size, which may give insight into which volcanic settings may be susceptible.

4. Methods

4.1 Introduction to methods

The overall aim of this project is to determine whether bubbles behave differently during shaking and what variables, shaking or systemic, are involved. The results will later be applied numerically and theoretically to see how natural systems may be affected. Behavioral changes include increased or decreased rate of rise and shape or size changes (e.g. Candela et al., 2014; Manga & Brodsky, 2006; Crews & Cooper, 2014). The methods used were developed using approaches from past experimental work and data from similar research. I have used field recorded earthquake data and previous shaking experiments to inform the parameters of shaking induced on the bubbles in the fluid (e.g. Crews & Cooper, 2014; Housener, 1963; Housner, 1957; Namiki et al., 2015). The fluids and bubbles used were determined using magmatic properties, rheology and data based on previous analogue experiments as laid out in the literature review (e.g. Cross, 2012; Galland et al., 2015; Merle, 2015; Taddeucci et al., 2006).

The variables tested were chosen to understand which aspect of seismic interaction and magmatic parameters may control how the behavior of bubbles changes, using the following variables;

- Systemic parameters
  - Viscosity of the viscoelastic fluid (Pa s)
  - Bubble size (mm)
- Shaking parameters
  - Duration of shaking (seconds, *s*)
  - Displacement (mm)
  - Frequency of shaking (Hz)
  - Acceleration (*g*) due to shaking as a function of displacement and frequency where $g = 8.9$ m s^{-2} (Bueche, 1970).

Experimental work has been carried out at the German Helmholtz Research Centre for Geosciences (GFZ) Potsdam, Germany, and most of the data analysis was carried out at the University of Canterbury, Christchurch, New Zealand.

4.2 Equipment, Sensors, Materials, Methods and Parameters

4.2.1 Shaking table and tank

To simulate seismic shaking a Geo-SIG GSK-166 Uniaxial Linear shaking table was used, which imposed horizontal oscillations on the fluid filled tank (Fig. 1). This table has been used in previous of investigations the effects of earthquakes on volcanic systems (Namiki et al., 2016) and to test seismic intensity meters (Xin et al., 2014). The shake table is capable of a linear stroke, both horizontal and vertical, up to 660.0 mm with a maximum velocity of 4.8 m/s and a maximum acceleration of 3.0 *g* (GeoSIG Ltd, 2009). The oscillations can be programed and controlled using GeoDAS software. Oscillations induced using this are repeatable and accurate.

The shake table parameters run were chosen to show a range of seismic scenarios to understand the conditions bubbles may change behavior (Ardeleanu et al., 2012; Murphy & O'Brien, 1977; Wald et al., 1999). These specific shaking parameters for each experiment are given in section 4.4. All experiments were run with the Geo-SIG GSK-166 set for producing horizontal oscillations.

A tank with the dimensions 240 x 85 x 235, and a volume of 4.79 L, was attached to the shaking table platform. The tank had two small sealable ports on the side three cms above the base of the tank, through which bubbles were injected. This tank was selected to use as it was the largest available with lower injection ports. Benchmark experiments which tested fluid stability detected no sloshing of the viscoelastic fluid during shaking (Namiki et al., 2016). Sloshing has been reported to be an issue with lower viscosity fluids. However, the viscosities used in these experiments were high enough to negate sloshing effects. The larger size of the tank also negated edge effects which may have led to issues with bubble behavior (Chen & Nokes, 2005; Frandsen, 2004; Housener, 1963). Neither sloshing nor edge effects were noted in the benchmark experiments for this project.

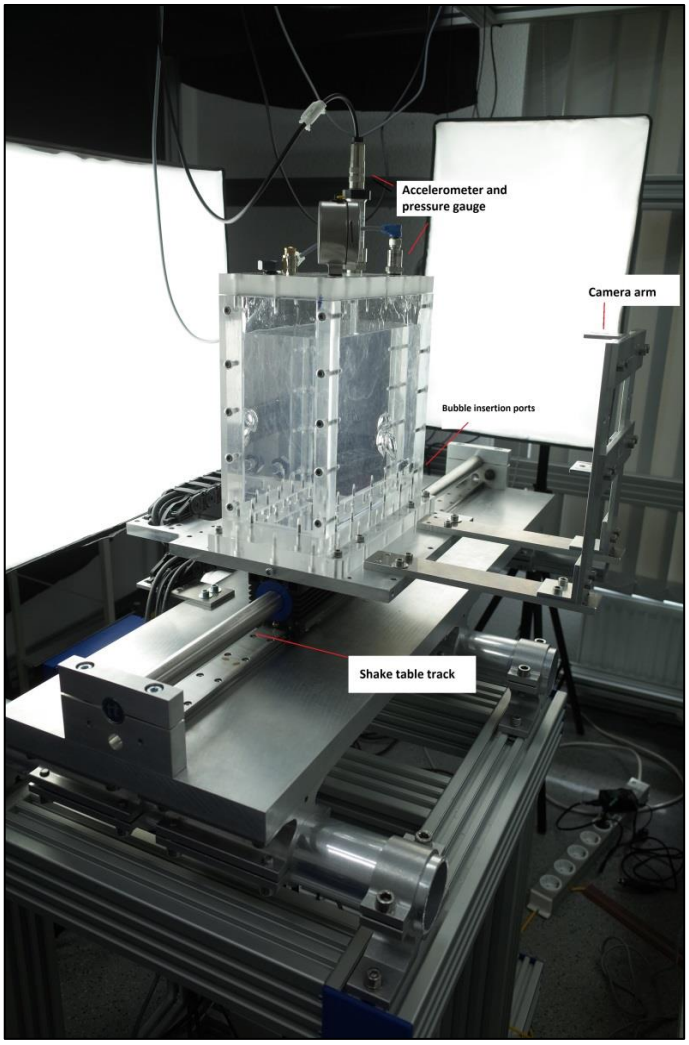

Image 1. Photograph of the experimental apparatus setup. Geo-SIG GSK-166 shaking table with camera arm and lighting.

On the back of the tank a transparent 10 x 10 mm grid was placed as a scale for bubble movement analysis. The grid covered only half of the back of the tank and the bubble was injected into the area not backed by scale grid. This method meant that it could be used for scale analysis but would also leave the area behind the bubble clear for computer analysis (Del Bello et al., 2012).

4.2.2 Recording and monitoring

The experimental set up also consisted of recording, monitoring, and lighting sensors and equipment. These were used to record the acceleration of shaking, and pressure and temperature changes within the tank. These devices were located on or in the lid of the tank. Each experiment was filmed for later analysis of bubble behavior. These sensors were recorded using Bubble Lab, software which was developed at GFZ for bubble shaking experiments (Namiki et al., 2016).

4.2.2.1 Accelerometer

Acceleration of the tank during shaking was measured using an Omega ACC103 laboratory accelerometer. This sensor is capable of measuring and recording frequencies from 1 Hz to 10 kHz with a mounted resonance frequency of >40 kHz and at a maximum g of ±1000 g, without clipping. It is suitable at temperature ranges from -50 – 120º C.

4.2.2.2 Pressure sensors

Pressure was recorded during the experiments so that the possible effects of advective overpressure due to bubble rise may be recorded. This was recorded using a Keller Highly Precise Pressure Transmitter, series PR33X / 80794. This measures pressures from 0.8 to 1,000 bar at a resolution of 0.002 % FS.

4.2.2.3 Thermometer

Temperatures were recorded during the experiments as the silicon oils used have a temperature dependent viscosity, although it is relatively stable at normal ambient temperatures (Obermeier, 2015). Temperatures were recorded using an Endress + Hauser Easytemp TMR31 compact thermometer, which operates accurately from -50º-200º C. This is well within the range of this project.

4.2.2.4 Camera

All filming, of both calibration and the experiments, was carried out using a Ricoh GRII camera. This camera has a Ricoh GR f/2.8 fixed lens, equivalent to 28mm, and 16.2 MP APS-C CMOS sensor. Video recording was shot at full HD 1080p at 30 fps (Hakala et al. 2010). Issues arose with automatic focusing during shaking and resulted in out of focus images post-processing. To mediate this, focus was set manually so that the bubble was in as clear a frame as possible, despite shaking and lighting changes. The camera was affixed to the arm attached to the tank. However, some wobble of the camera on the arm occurred during shaking. This was corrected post-filming and the methods used to analyze took this into consideration.

4.2.3 Viscoelastic fluid as magmatic analogue

In the shaking experiments for this project Korsilon oil was used. This is a transparent, viscoelastic silicon oil produced by Obermeier for industrial purposes (Obermeier, 2015). Three different viscosities were chosen for the experiments; 2,000 Pa s, 10,000 Pa s, and

30,000 Pa s. The 10,000 Pa s was made specifically for this project and so does not appear within Obermeier rheology data. The silicon oils have low surface tension, and are highly incompressible. The fluids behave as both Newtonian and non-Newtonian fluids, dependant on shear rate. Their viscosity is dependent on shear strain rate, similar to magmas (Giordano et al., 2008; Dingwell, 2006; Lejeune et al., 1999). These viscosities were chosen as they portray a range of intermediate viscosity magmas, (Fig. 2) (Spera, 2000; Giordano et al., 2008). The viscosity of the silicon oils has a low temperature dependency (Fig. 3). However temperature was recorded during the experiments to verify stability. The silicon oils also have a relatively high shear rate stability, making them ideal for shaking experiments, (Fig. 3) (Llewellin et al., 2016). All three fluids used for this project have a density of 0.97 g/cm³, the complete rheological details are given in Figure 4.

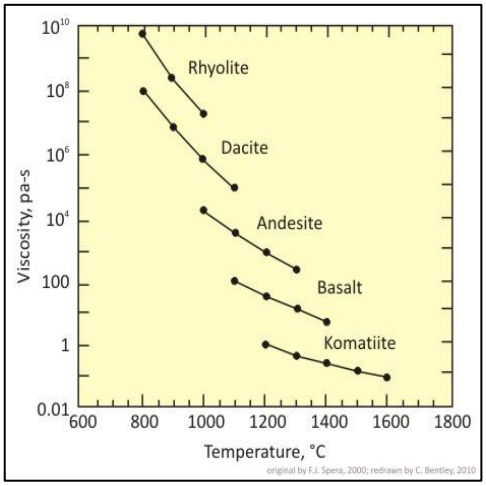

Figure 1. Magma viscosity range (Spera, 2000).

The silicon oils used are produced for industrial purposes by Obermeier, and so the given rheology is considered accurate. Several attempts were also made to check viscosity through several equations which define the velocity of bubble rise related to their diameter and the viscosity of the fluid, based on variations of Stoke's Law (Baz-Rodríguez et al., 2012). However, these methods did not prove useful as different equations are necessary for bubble size ranges and previous work into this is not comprehensive. It should be noted that Obermeier gives viscosity in mPa s but for the purpose of this thesis it is given in Pa s.

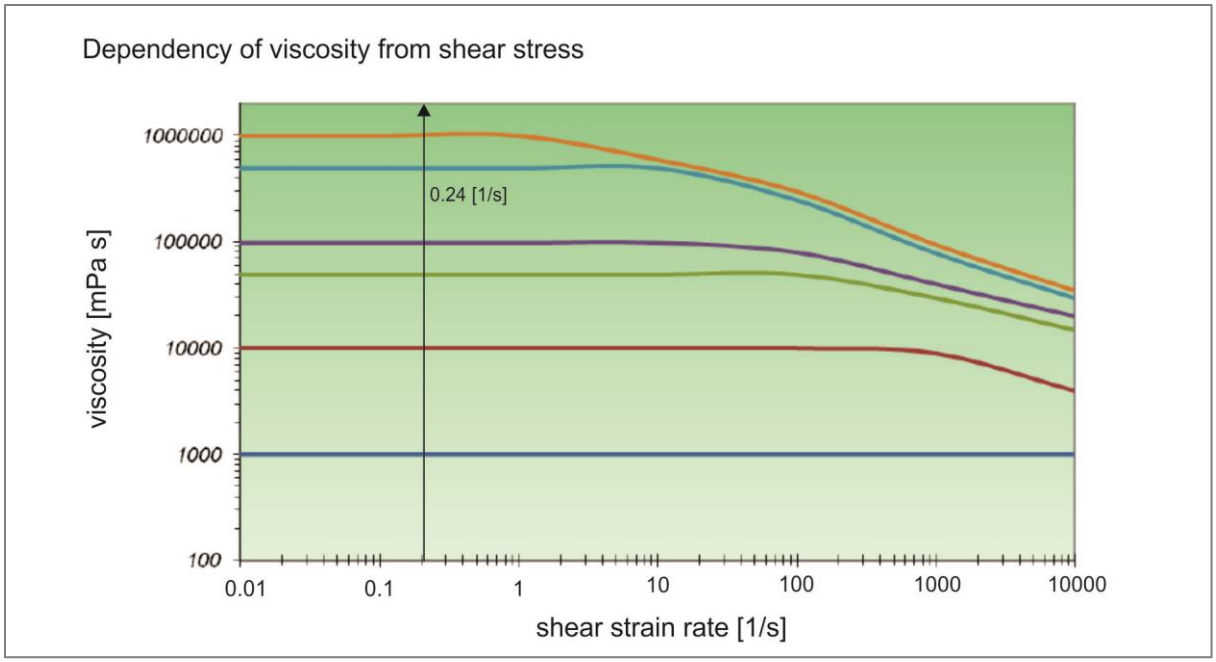

Figure 2. Dependency of viscosity based on shear strain rate.

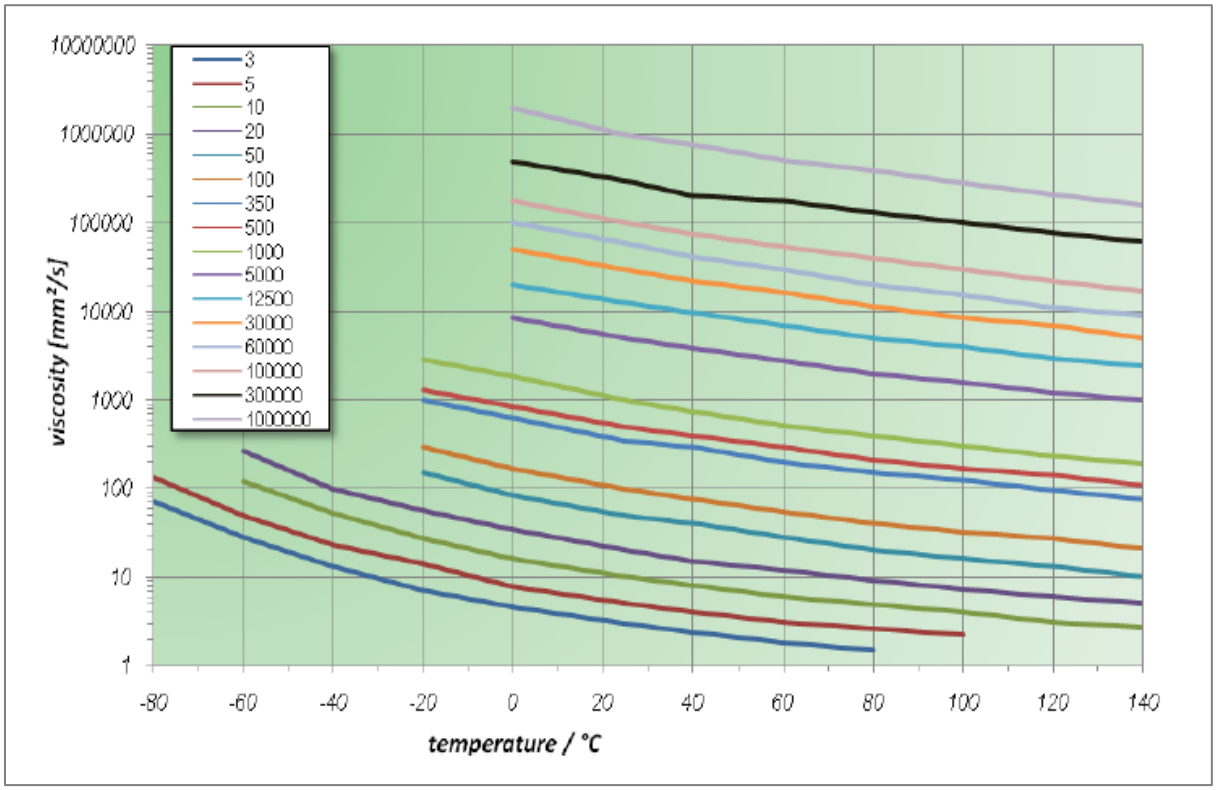

Figure 3. Viscosity of silicon oil based on temperature.

KORASILON Öl M	Viscosity bei 25 °C	Specific gravity at 25 °C	Heat expansion coefficient from 0 - 150 °C	Thermal conductivity at 50 °C	Flash point	Pour point below	Refractive index at 25 °C	Dielectric constant at 25 °C and 10^2 Hz	Surface tension at 25 °C
	[mm²/s]	[g/cm³]	[10^{-4}cm³ / cm³ °C]	[W / K x m]	[°C]	[°C]			[mN/m]
0,65	0,65	0,76	13,4	0,10	-4	approx. - 70	1,375	2,18	15,9
1	1	0,82	12,9	0,10	approx. 30	approx. -86	1,382	2,28	16,9
2	2	0,87	12,4	0,11	75	approx. -120	1,319	2,30	18,3
3	3	0,90	11,1	0,11	> 62	approx. -100	1,394	2,40	18,9
5	5	0,92	10,8	0,12	> 120	approx. -100	1,396	2,49	19,2
10	10	0,93	10,0	0,13	> 165	approx. -90	1,399	2,61	20,2
20	20	0,95	9,7	0,14	> 200	approx. -70	1,401	2,68	20,6
50	50	0,96	9,5	0,14	> 250	approx. -55	1,402	2,69	20,8
100	100	0,97	9,4	0,15	> 275	approx. -55	1,403	2,71	20,9
350	350	0,97	9,3	0,15	> 300	approx. -50	1,4035	2,73	21,1
500	500	0,97	9,3	0,15	> 300	approx. -50	1,4035	2,74	21,1
1 000	1 000	0,97	9,2	0,15	> 300	approx. -50	1,4035	2,74	21,2
5 000	5 000	0,97	9,2	0,15	> 300	approx. -50	1,4035	2,74	21,4
10 000	10 000	0,97	9,2	0,15	> 300	approx. -45	1,4037	2,75	21,5
12 500	12 500	0,97	9,2	0,15	> 300	approx. -45	1,4037	2,75	21,5
20 000	20 000	0,97	9,2	0,15	> 300	approx. -45	1,4037	2,76	21,5
30 000	30 000	0,97	9,2	0,15	> 300	approx. -45	1,4037	2,76	21,5
60 000	60 000	0,97	9,2	0,15	> 300	approx. -45	1,4037	2,76	21,5
100 000	100 000	0,97	9,2	0,15	> 300	approx. -40	1,4037	2,76	21,5
300 000	300 000	0,97	9,2	0,15	> 300	approx. -40	1,4037	2,76	21,5
500 000	500 000	0,97	9,2	0,15	> 300	approx. -40	1,4037	2,76	21,5
600 000	600 000	0,97	9,2	0,15	> 300	approx. -40	1,4037	2,76	21,5
1 000 000	1 000 000	0,97	9,2	0,15	> 300	approx. -40	1,4037	2,76	21,5
2 000 000	2 000 000	0,97	9,2	0,15	> 300	approx. -40	1,4037	2,76	21,5
G 30 M	30 000 000	0,97	9,2	0,15	> 300	-	1,4037	2,76	21,5

Figure 4. Properties of silicon oil used in experiments (Obermeier, 2015). 2,000,000 mPa s corresponds to 2,000 Pa s and G 30 M corresponds to 30,000 Pa s. 10,000 Pa s does not appear in the data as it was made specifically for this project.

4.3 Benchmark experiments and procedures

4.3.1 Basic experimental preparation procedures

The tank was filled 20 mm from the top to protect the sensors located in the lid. The fluid had an overall depth of 220 mm. When filling the tank remnant bubbles were incorporated during pouring. To remove remnant bubbles the fluids were simply left in the tank overnight and the bubbles were allowed to rise and escape. Experiments with 2,000 and 10,000 Pa s contained no remnant bubbles. However, the rate at which bubbles < 1 mm in diameter rose in the 30,000 Pa s fluids meant that the fluid took too long to fully clear of artifact bubbles. This problem was negated by injecting several very large bubbles into the tank and allowing them to either coalesce with, or push aside the small remnant bubbles. This way a path was cleared for the experiments to take place, uninfluenced by small bubbles which might affect bubble behavior.

Injection of air bubbles into the fluid was done using a graduated syringe affixed with a 200

mm long needle. Air bubbles, which have a density of 1.225 x 10^{-3} g/cm^3, were used for all of the experiments. Three different size bubbles were tested in the experiments; 15, 20, and 25 mm, with volumes 17.7 mL, 41.9 mL, and 81.8 mL calculated using the formula $V = 4/3\pi r^3$ (Lang 2009).

Bubbles in volcanic systems occur in a very wide range of diameters (Huppert & Woods, 2002; Parmigiani et al., 2016; Kedrinskii et al., 2005). These sizes were chosen as they were large enough to travel a distance which would be able to be recorded in a reasonable timeframe. Yet the rise velocity of these size bubbles was not so high that conducting experiments in the 2,000 Pa s would rise too fast to accurately run.

4.3.2 Calibration of bubble sizes in experiments

In order to verify the diameter of the bubbles injected calibration files were made. All filming, of calibration and the experiments, was done using a Ricoh GRII camera. This was done by inserting a stiff metal measuring tape into the liquid, through the port at which bubbles were injected (Del Bello et al., 2012). An image of this was then overlain with one of the bubbles in experiments using Adobe Photoshop so that the horizontal diameter of the bubble could be measured accurately. Experiments in which bubble size was either too large or too small were not used for analysis. The method of injection used was typically found to be accurate to 0.2 mm. Verifying this measurement was particularly important for the 30,000 Pa s fluids. Because of the stiffness of the fluid, air back flowed out through the injection point if enough time was not taken to allow the fluid to relax back around the needle before withdrawing.

4.3.3 Benchmark experiments with still rise bubbles

Before beginning shaking experiments a series of benchmark experiments were run. These aimed to do several things. First, it was to test injection methods and to determine the accuracy of the air bubble size when injected, as discussed in section 4.3.2. Second, the velocity of a single, rising bubble without the influence of shaking was observed and recorded. This was done by injecting a bubble of a given size into the tank with a 10 x 10 mm grid on the back. Filming began with injection as the shape of the bubble and how it developed was also of some interest. The bubble was then allowed to rise to the top of the tank. Using the video I then calculated the amount of time which the top of the bubble took to

cross the gridlines in order to get the time it took to traverse a given distance from 10-80 mm. This was then used to determine bubble rise rate in cms per minute. The time it took to travel 10 mm was recorded at the beginning, middle, and end of its upwards rise. This was done to determine how long it took for a bubble to reach its maximum velocity as well as to see if there was a discernible change in velocity as the bubble rose closer to the surface of the fluid and pressure decreased. This gave us the range of rise area in which experiments could be run without being affected by injection or vicinity to top of the fluid.

Calculations of bubble rise velocity (u) were carried out and results were compared to the actual rise velocity observed. Several different formulas were tested to see if rise speed could be determined and used to verify viscosity measurements. However only the following from Parfitt & Wilson (Parfitt & Wilson, 2009), was found to be anywhere near the actual rise speed;

$$u = [(2/9)(\Delta p)(g)(r^2)]/\eta \quad \text{(Parfitt \& Wilson 2009)}$$

Where u is the velocity, Δp is the change is the density change (density of fluid-density of the gas, km/m^3), g is the acceleration of gravity, r is the radius and η is the fluid viscosity. The results derived from this formula were relatively accurate but not enough to be used for the purpose of this project. The difficulty with using this formula or another similar formula, is that bubble surface area and the drag it creates, is paramount for accuracy, according to Stoke's Law (Chhabra, 2006; Talaia, 2007). Different formulas are required for differing bubbles sizes and viscosities. While it is calculable, determining the formula to use is not necessary for this project. Observed bubble rise velocity has been considered far more accurate and so was used for analysis in this project.

4.4 Shaking Experiments

The shaking experiments were designed and carried out in a way to answer the questions set out in the beginning of this section and in a way that was repeatable for the best results. The primary experiments for this project were conducted with a single bubble. Several experiments were also involved two bubbles coalescing, both without shaking and during shaking. However, these proved to be very difficult to carry out with reliable repeatability and were therefore not included within the scope of this project. Data from these experiments may be of interest for future work.

A total of 84 different experiment parameters were run. Three different viscosities were tested; 2,000 Pa s, 10,000 Pa s, and 30,000 Pa s. Three different bubble sizes were tested; 15 mm, 20 mm, and 25 mm. Eleven different shaking parameters were chosen, as shown in Table 1, to test duration (seconds), displacement (mm), and frequency of shaking (hertz). These parameters resulted in shaking with accelerations (g) ranging from 0.04 g to 0.95 g.

Table 1. Shaking experiment parameters. Gives the duration, displacement, frequency, and acceleration of each experiment. The experiment code is how the parameters are referred to throughout the thesis.

Code	Duration (seconds)	Displacement (mm)	Frequency (Hz)	Acceleration (g)
E1	2	20	1	0.11
E2	2	20	3	0.47
E3	2	120	1	0.05
E4	2	120	2	0.04
E5	30	20	1	0.12
E6	30	20	3	0.43
E7	30	120	1	0.33
E8	30	120	2	0.95
E9	30	160	1.6	0.95
E10	60	20	4	0.73
E11	60	160	1.6	0.94

Once the tank was filled with a fluid, the lid emplaced, and artifact bubbles had been cleared a single bubble was injected through the lower side port. When being injected the tank lid port remained open to avoid pressure measurements being influenced by new bubble injection. The top port was shut after bubble injection. The bubble was allowed to fully form as following injection they retained a remnant tail from the needle pulling back and out of the tank. After waiting for the bubble to reach its terminal still velocity the camera began filming. The bubble was recorded in a non-shaking rise for approximately 1½ - 4 minutes, depending on fluid viscosity so that behavior before shaking could be observed for each experiment. More viscous fluids were filmed for longer before and after shaking as bubbles travel much slower in these (Talaia, 2007). Shaking was then initiated using GeoSig software (GeoSIG Ltd, 2009). Filming continued throughout the shaking and again for 1½ – 4 minutes after shaking had finished to record behavior post-shaking.

For 2,000 Pa s viscosity experiments the bubble was allowed to rise and escape before another experiment took place. However, for 10,000 Pa s and 30,000 Pa s viscosity experiments the bubble was allowed at least a two minute rest period and then another experiment was run using the same bubble. In between each of these experiments the lid port was reopened to reset the pressure within the tank. The reuse of bubbles in these experiments was done for expediency of the experimental process.

4.5 Analysis of bubble rise velocity, pressure, acceleration

4.5.1 Methods for bubble rise analysis

The resulting data included the recorded video of the experiment and Bubble Lab data, exported as a Microsoft Excel spreadsheet. The Bubble Lab data gives the pressure changes, temperature, acceleration, and duration of shaking on a millisecond scale. Recording of these measurements only occurred during operation of the shaking table and so does not correspond exactly to the video taken. Analysis of this material was carried out using Microsoft Excel and ImageJ software (Rasband, 2015), MTrackJ (Meijering et al., 2012) and Image Stabilizer (Li, 2008).

Before bubble analysis began several conversions and corrections were made of the video. First, they were converted into one image per two seconds using Adobe Premier Pro. It was chosen to film the experiments, instead of taking one image per second using the camera, so that the option was available to use either the video or images for analysis. One image every two second ratio was chosen so that bubble rise for all three viscosities could be tracked accurately. At one image per second tracking bubble rise in the 30,000 Pa s fluids became inaccurate as rise velocity was not fast enough.

A slight wobble was detected in the experiments E6 - E11, caused by a slight movement of the camera on its boom during shaking at higher velocities. The wobble is, at most, a millimeter of horizontal movement. However, as bubble movement occurs on similar scale all care was taken to correct this prior to rise analysis. This was attempted on both the film and images stacks. While multiple methods were tested ImageJ plugin, Image Stabilizer was found to be the most effective (Li, 2008).

Attempts were made to correct the video itself, before being converted into images, using Adobe After Effects image stabilization. This process proved to take longer than was feasible for the scope of this project and little to no change was seen in the wobble. Likewise, Adobe Photoshop image stack stabilization was tested on several image sequences. No change was seen using this method and again the process was time consuming with the large amount of images within each image sequence. However, ImageJ software was several plugins used for image stabilization. ImageJ Template Matching (Rasband, 2015) required each image stack to be converted to an 8-bit or 16-bit grayscale tiff file before analysis. This was carried out using Adobe Photoshop. The resulting image sequences were not improved. Instead image stability

was made worse in several instances. This is likely because the grayscale was not stable on a single point throughout the image stack due to the changing light during shaking. Light changes occurred because the photography lights behind the tank remained stationary while the tank shifted position.

ImageJ Image Stabilizer (Li, 2008) was the most efficient and effective method tested and was therefore utilized for correcting the image sequences before analysis took place. Some remnant wobble may remain as correction was not entirely accurate but the method used for analyzing bubble rise rate negates the need for perfect wobble negation.

4.5.2 Tracking bubble edge movement

The bubble in the corrected image sequence was then analyzed using ImageJ plugin MTrackJ (Meijering et al., 2012). This plugin allows the user to track the movement of an object from image to image and then exports the overall changes in position as a Microsoft Excel spreadsheet. In the first image two scale points were emplaced, 100 mm apart, using the gridlines on the back of the tank. Then the top edge of the bubble was zoomed in on and a spot on it was chosen to track through the sequence. Typically, a spot on the left top edge was chosen, where the pixels began to descend down the curve of the bubble. This region of the bubble proved the easiest area to track reliably. Tracking of the chosen spot on the bubble curve became more difficult during shaking as the lighting did not move with the shaking platform and camera, causing a shift in light across the bubble.

While tracking the movement of the bubble edge and movement away from the normal velocity of rise was detected care was taken to zoom out and check for camera movement or focusing issues. These issues may cause bubble movement which, when zoomed in, looked like increased upwards velocity. In cases where this was the case the image sequence was discarded and another used in order to negate this corrupting the velocity data.

The resulting Excel spreadsheet was then used to produce a graph comparing non-shaking rise to possible changes in rise velocity during shaking. First, using the 100 mm scale set at the beginning of the difference between pixel (x) and pixel (y) was calculated. The pixel difference was then divided by 10 cms (100 mm converted for scaling) to get a scaling ratio. Then the pixel difference is multiplied by the scaling ratio to give movement of the bubble graphed temporally on a cm scale. Each point on the graph corresponds to bubble movement every two seconds. Tracking bubble movement every two seconds allowed for the most

accuracy for all viscosities, as mentioned in section 4.5.1.

In order to determine if there are deviations from the still rise velocity behavior the points have been divided into; pre-shaking, shaking, and post-shaking (Fig. 5). This is done using the Bubble Lab data and the times at which shaking begins and end, as seen in the experiment video. Points subject to shaking have been highlighted in red. A linear trend line has then fitted to the pre-shaking data. Bubble movement deviation from the pre-shaking trend line is calculated and plotted as the trend line of deviation. From this any deviations from the normal rise velocity may be seen. The experiments chosen to portray have the same system parameters and duration but different shaking parameters.

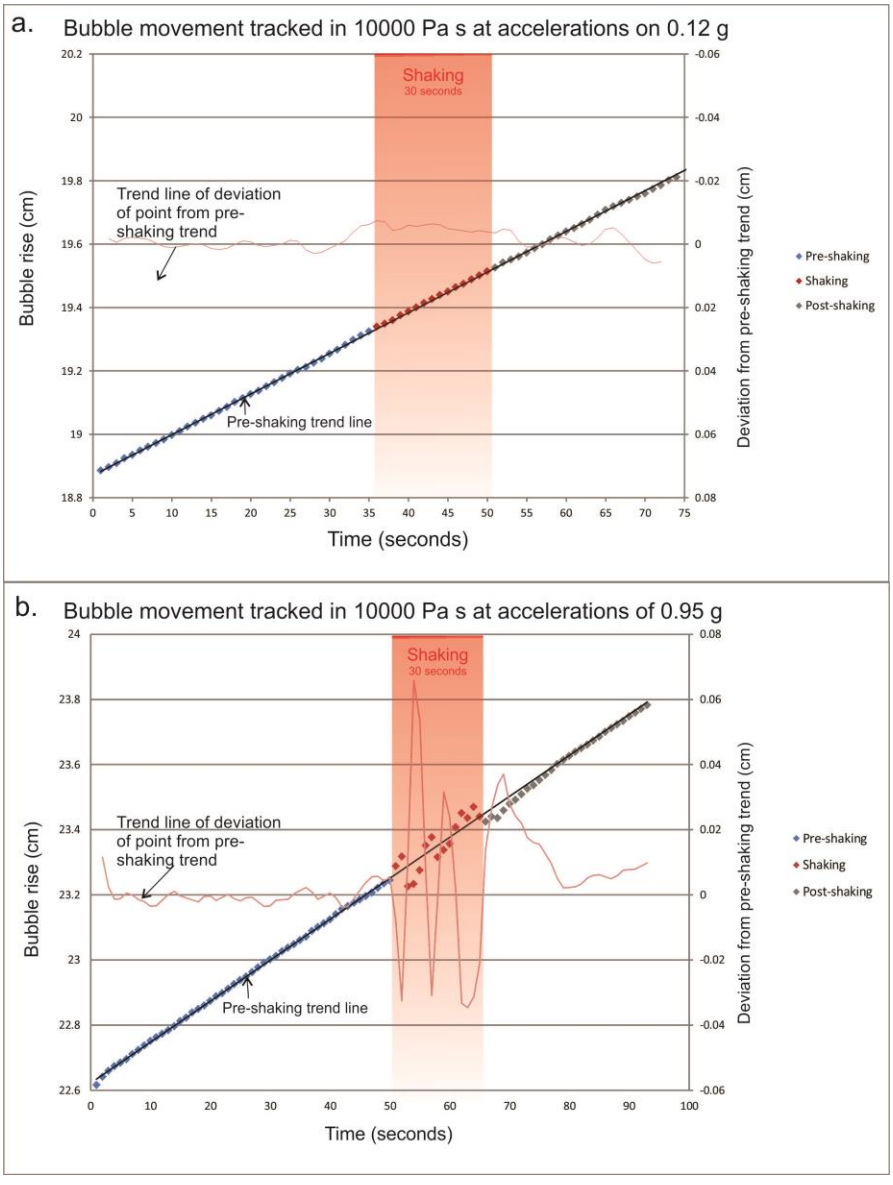

Figure 5a-b. Tracking of bubble pre-, syn-, and post-shaking. Graphs show a comparison of two shaking experiments and the amount of bubble movement for each. Each point represents upwards movement of the bubble with a trend line affixed to pre-shaking movement. A second (red) trend line shows how much each point deviates from the pre-shaking trend. This highlights amount of bubble movement during shaking.

4.5.3 Analyzing bubble rise velocity

The change in velocity of a bubble during shaking was determined using a similar technique in ImageJ using MTrackJ. Instead of tracking bubble movement for each frame it was tracked from the start to finish of shaking and then for an equal amount of time of non-shaking. This gives the difference in distance travelled between non-shaking and shaking. A scale was created using the grid on the back of the tank. This created a 10 mm scale bar, as opposed to 100 mm, as that distance was determined to be more relevant to the calculations needed. The bubble was then tracked during a still rise for the same amount of time as the duration of shaking for that experiment. Only two points were placed for this travel time, at T_1 and T_2. This procedure was then repeated for the time spanning the duration of shaking. The first point, Shaking T_1, was placed on the frame in which shaking began and the second on the frame in which shaking ends, Shaking T_2. Using the same method as previously explained, the 10 mm scale bar has been used to calculate a scaling ration and then determine the distance travelled by the bubble from T_1 to T_2. The difference between these two distances and that difference has been turned into a percentage. I have used percentages of the difference so that all of the experiments could be compared, despite the distance differences due to viscosity and bubble size being considerable. This method of calculating changes in velocity has the added benefit of not being affected by any artifacts of camera shaking.

Using the percentage of difference from still rise the rate increase is calculated. This was done by using the still rise velocity calculated using video of bubble rise and the 100 x 100 mm grid on the tank. This process is explained in the benchmark experiment section.

Error bars for the percentage difference of still rise to shaking rise velocity was calculated using repeat experiments. The process of working out the difference in rise velocity was repeated using nine additional, repeated experiments. Nine experiments were used; one of each bubble size, from each viscosity. Shaking parameter E8 was chosen as it had a high acceleration, g, and experimental repeats were of good quality. The differences were averaged and used as a fixed error bar of 0.48 for results.

4.5.4 Bubble shear analysis

During shaking a shearing of the bubble could be seen (Fig. 6). In order to determine whether this was true bubble movement or an artifact of camera wobble a shape comparison overlay has been made. This was done by selecting a series of images, one every two seconds. In the

first image the bubble edge has been selected and the bubble colored red. This acts as the base image against which all others are compared to. Each consecutive bubble is then cut from its image and overlain onto the primary base bubble. The consecutive bubble is lined up with the base bubble using the tail of the bubble, as this remains the most stable and results in a more accurate overlay. This is done as a separate image for each bubble in the series. The changes in bubble morphology can then been seen as the differentiation from the red to the grey-scale bubble which is overlain.

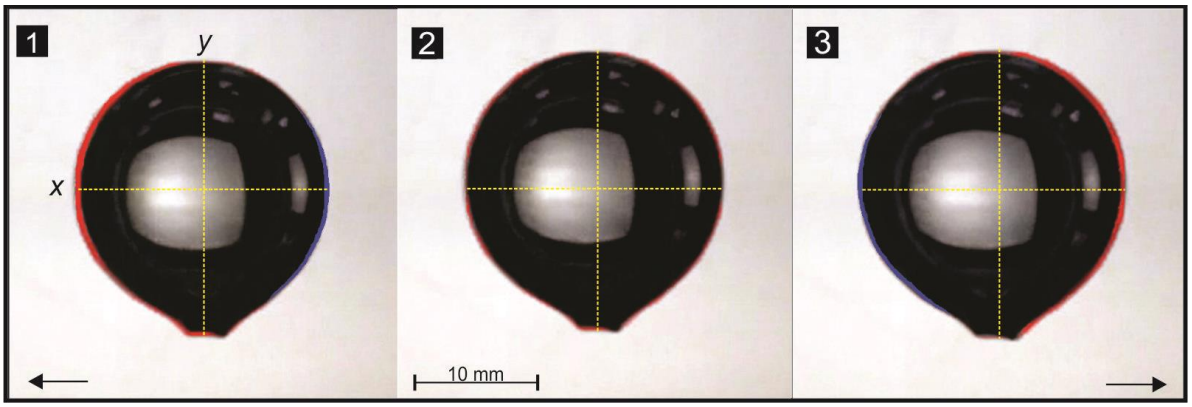

Figure 6. Bubble overlay showing shear during shaking. The bubble underneath has been coloured red. Where bubble shear has occurred the red is exposed beneath.

Attempts to measure the surface area and diameter of the bubble were also made to see if volume changes occurred. However, the resolution of the images was not fine enough to measure this with any accuracy. Further work for this field would benefit from running similar experiments with higher resolution and high speed cameras to accurately determine the changes happening to bubble morphology during shaking. Determining contraction volume changes has implications of cavitation (Plesset & Prosperetti, 1977) and rectified diffusion processes (Ichihara & Brodsky, 2006).

5. Limitations

While this project does illuminate the possible effects of shaking on magma chambers it is not without limitation and sources of error. Volcanic systems are stochastic and difficult to model. The limitations of this project are considered here and some suggestions for further work made.

In the experimental section of this project the resolution used was not fine enough to carry out some calculations which may have been interesting to note. I suggest that if further work was done in this area that high-speed, higher resolution filming be used. This may allow further work to determine whether bubble volume changes are occurring and give better insight into the mechanism which increases rise rate.

More accurate and broader rheology data is needed on the silicon oil used for this project in order to determine to what extent viscosity is affected by shaking. The data set given by Obermeier (2015) gives shear strain rate viscosity dependency to viscosities up to 1,000,000 mPa s, or 1,000 Pa s. The lowest viscosity used for this project was 2,000 Pa s. It can be assumed that viscosity was lowered but not to what extent this occurred.

Both the experiments and calculations carried out for this project are based on a two-phase system of fluid and gas, without the presence of crystal matter. They are also based off of a single bubble system. Bubble behave differently in the presence of crystal matter (Parmigiani et al., 2016) and other bubbles (Baz-Rodríguez et al., 2012; Parmigiani et al., 2016; L'Heureux, 2009; Llewellin et al., 2016).

Similarly, the advective overpressure calculations do not take into account volume of bubble and system. Nor do they consider compressibility or pressure regimes (Pyle & Pyle, 1995; Sahagian & Proussevitch, 1992). Bagdassarov (1994) makes a heated argument against this and has offered a more comprehensive calculation for advective overpressure (Bagdassarov 1994). However, for the scope of this paper it was determined that the calculations used were sufficient to demonstrate that shaking may lead to higher increases in pressure.

Volcanic systems are stochastic, and modelling their behaviour always provides challenges and difficulties (Galland et al., 2015). While these limitations exist I do not believe that they take away from the overall results of this project. My study provides several interesting areas that significantly expand the field of volcano-tectonics interactions particularly relevant.

6. Results

6.1 Overview of experimental phenomena

Pre-shaking bubble rise showed a constant rise rate, according to viscosity and bubble size (Baz-Rodríguez et al., 2012). On shaking, rise rate increased, correlating with a shear in bubble shape. Bubble rise rate returned to pre-shaking rise rate upon cessation of shaking. The results of the experiments show that bubbles increase their rise velocity from 1.91 % to 13.33 %. Higher increases in shaking rise rate appear to correlate positively with increased shaking acceleration, but have no apparent relationship to fluid viscosity, bubble size, or displacement. The full results have been presented in Figure 7a-d, given as the percentage of difference from non-shaking to shaking distance travelled. Methods for obtaining the percentage of rate difference have been given in Section 4.5.3. Full parameters and results of the experiments are given in Appendix, Table 7.

6.2 System and shaking parameters: viscosity, bubble size, and displacement with no measurable effect.

When averaged, bubble rise rate increased by 6.20 %. The experiment which showed the highest changes in rate of upwards rise involved the 10,000 Pa s fluid, 20 mm bubble, and 120 mm displacement of shaking with accelerations of 0.95 *g*. The experiment which resulted in the lowest change of rate was 2000 Pa s, 25 mm bubble, 120 mm displacement of shaking and an acceleration of 0.33 *g*. Viscosity, bubble size, and displacement of shaking does not appear to have a direct effect on the increased rate of rise of a bubble during shaking. While frequency (Hz) was an input parameter for shaking it has not been presented as a variable except when connected to displacement, giving acceleration.

6.2.1 Bubble size

When the results are looked at according to bubble size there is no discernible trend seen (Fig. 7a). Table 2 shows the lowest and highest rate increase for each bubble size, and the given average for each of these. Data shows that the average and lowest increase in rise rate for each bubble size decreases slightly with bubble diameter increase. The highest rate changes are all very similar.

Table 2. Results from bubble size.

Bubble Size (mm)	Lowest rate change %	Highest rate change %	Average rate change
15	3.69	12.95	6.84
20	2.12	13.33	6.18
25	1.91	11.37	5.66

6.2.2 Viscosity

Viscosity data plots also show no major trends or features, (Fig. 7b). The average change of rate for each viscosity does not show any trend either. The highest average change in rise rate is seen in 10,000 Pa s viscosity experiments, (Table 3).

Table 3. Results from viscosity.

Viscosity (Pa s)	Lowest rate change %	Highest rate change %	Average rate change
2000	1.91	11.61	6.20
10,000	3.29	13.33	6.53
30,000	2.12	12.95	5.87

6.2.3 Displacement

There was no discernible trend when looking at rise rate changes against displacement of shaking, (Table 4, Fig. 7c). Ranges and averages for long displacement are given in Table 4 both separate and together as 120 mm and 160 mm displacements were considered long displacement experiments, compared to short, 20 mm displacement. The lowest average change in rate is seen in short displacement experiments while the longest it seen in 120 mm displacement experiments. This is likely because acceleration for 20 mm experiments was only able to reach 0.73 *g*, due to equipment limitations.

Table 4. Results from displacement.

Displacement (mm)	Lowest rate change %	Highest rate change %	Average rate change
20	2.12	9.23	4.91
120	1.91	13.33	8.10
160	2.69	10.21	6.05
120 & 160	1.91	13.33	7.07

Further evidence for this can be seen in both graphs in Figure 5 in section 4.5.2. In Figure 5a, it shows accelerations of 0.12 *g*, deviation from the pre-shaking trend line is minimal (under 0.01 cm). In Figure 5b, which tracks a bubble during accelerations of 0.95 *g*, deviations from the pre shaking trend line are up to 0.07 cm. For these particular experiments rate of rise rose 3.29 % and 8.00 % respectively.

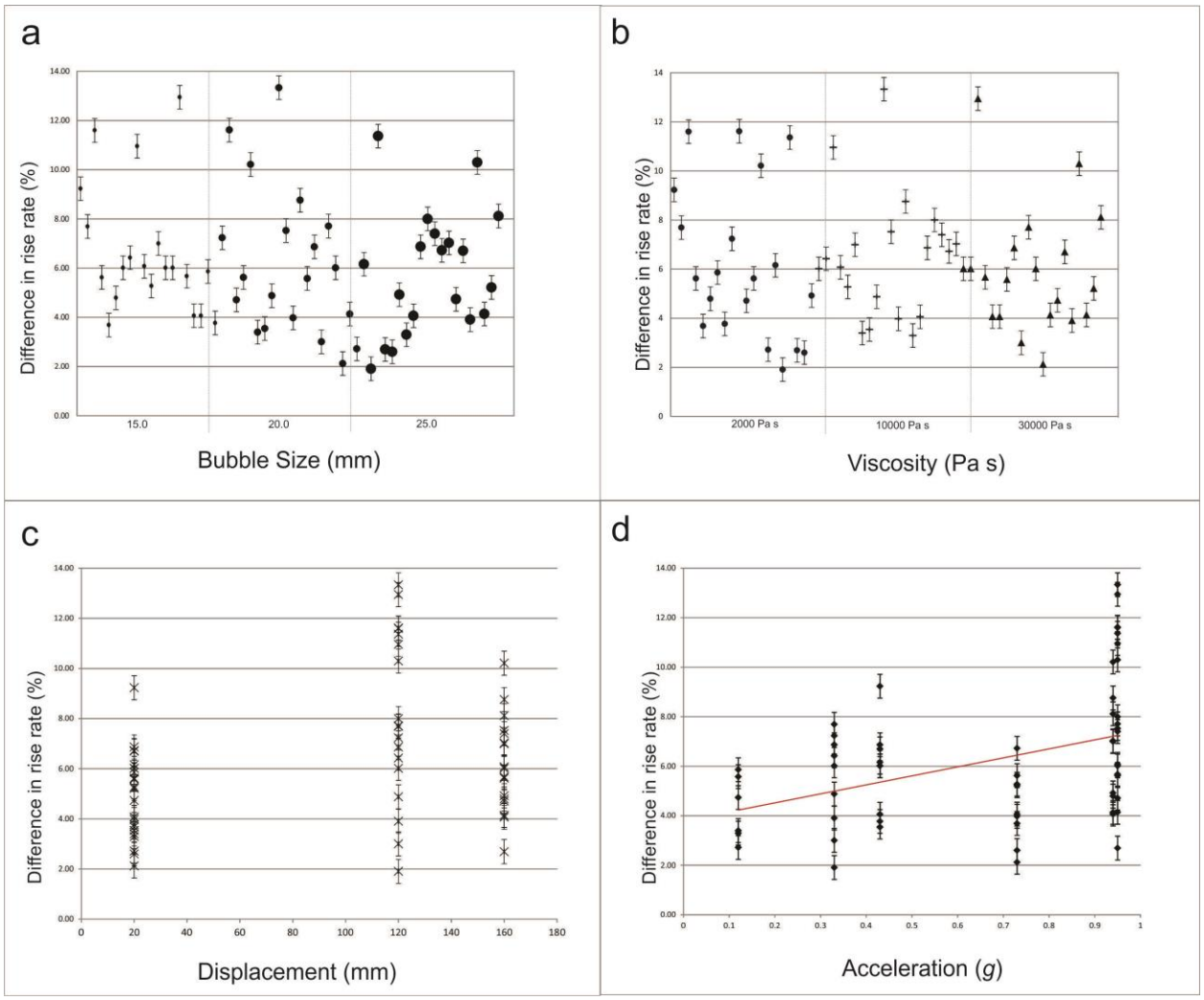

Figure 7a-d. Figure a. shows the range of results for bubble size. Figure b. gives viscosity, Figure c. gives displacement, and Figure d. shows results plotted with acceleration. A trend line has been fitted to acceleration as it is the only data set which shows a trend of any sort.

6.3 The measurable effects of acceleration on rise rate during shaking

Results from shaking experiments (Fig. 7d) showed a positive trend correlated to increased acceleration. The average acceleration increased for all accelerations except 0.73 g, which showed a decrease. However, the linear trend line, shown in red on Figure 7d, fixed to the full range of data plotted data continues to be positive. The two highest accelerations tested,

0.94 *g* and 0.95 *g*, are extremely close and so have been presented both together and separate, for clarity (Table 5).

Table 5. Results from acceleration.

Acceleration	Lowest rate change %	Highest rate change %	Average rate change
0.12	2.72	5.86	4.26
0.33	1.91	7.69	5.33
0.43	3.54	9.23	5.82
0.73	2.12	6.72	4.36
0.94	4.07	10.21	6.56
0.95	2.69	13.33	8.20
0.94 + 0.95	2.69	13.33	7.38

6.4 Bubble shear during shaking and the effects of duration

Changes to bubble behaviour appear to occur only during shaking. Much of the evidence for the effects of duration on shaking can be seen through bubble shear so these have been presented together. During shaking it was noticed that bubbles showed a shear that was not a remnant of camera shaking. Tracking the top of the bubble at a single point showed that the bubble moved not only horizontally but also vertically (Fig. 5). The shear was evident only during shaking and ceased immediately upon shaking ended, as far as is evident in the methods used. While tracking some bubbles there appeared to be a decay of velocity back to its pre-shaking speed this was not apparent in all, or even a majority. This is likely due to the difficulties in tracking bubble edge pixels in higher viscosities.

In Figure 5a-b (Section 4.5.2) each point represents two second intervals of upwards bubble movement, given on the left axis. A linear trend line has been fitted to the pre-shaking data. The deviation of each point from this trend line has been plotted as a second trend line, the trend line of deviation, given on the right axis. Pre-shaking, the deviation trend line is only slightly undulatory due to the difficulty in tracking a bubble top. In top graph during shaking a slight increase away from the left hand axis 0 line can be seen. The bottom graph, however, shows relatively strong movement away from the 0 line to approximately 0.07 centimetres difference from the pre-shaking trend.

Bubble shear is also evident in overlain images (Fig. 6). The series of three bubbles are overlie a pre-shaking bubble, with bubble aligned at their tails. Red shading shows the area that the deformed bubble no longer covers and the blue shading shows the additional area that

the blue bubble covers. Bubble 1 shows that during tank movement to the left the deformed bubble shears to the right. Bubble 2 shows the deformed bubble as the tank has just begin to move back in the opposite direction of shake, giving a fairly equant fit. Bubble 3 shows the top bubble shearing to the left as the direction of shaking moves to the right. Generally there is a greater area of red compared to blue that may indicate some contraction, although, the resolution limitations need to be emphasized. The fluid flow direction is opposite to the direction of shaking. This may be important for the mechanism of increased rate of rise and will be further discussed in section 6.4.3.

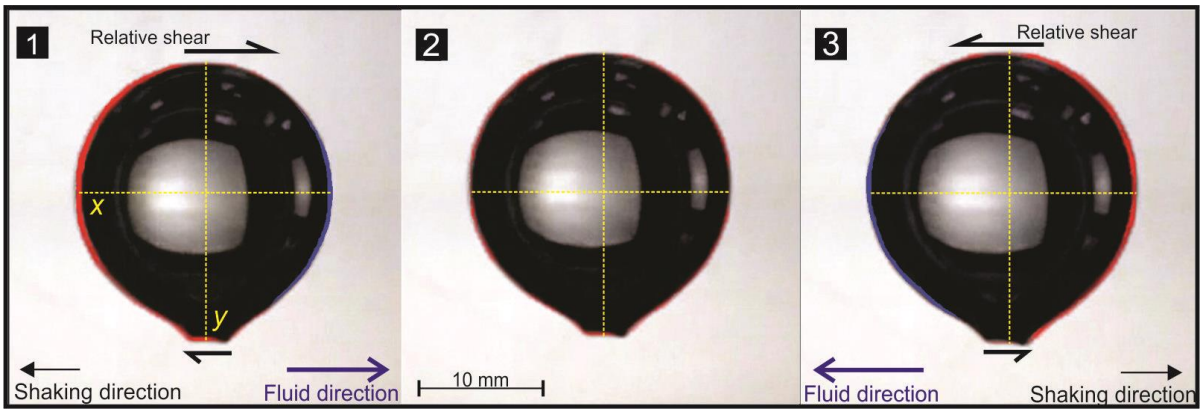

Figure 8. Bubble shear overlay. A bubble during shaking overlies a bubble pre-shaking. The underlying bubble has been coloured red so that changes of the top bubble due to shear can be seen. The black arrows show the direction of shaking. Blue arrows show the fluid movement direction caused by shaking. The half arrows on the top and bottom of the bubbles show the shear of the bubble.

6.5 Review of results

From the experiment results it can be seen that bubble behaviour, both rise rate and bubble shape, has been affected by shaking. Viscosity, bubble size, and displacement of shaking do not have a direct effect on the percentage of rise rate increase. The duration of shaking affects the bubble only while shaking is occurring, but does not appear to have a lasting effect and does not affect the percentage of rate increase. Acceleration does have a positive effect on increased rate rise with increased rate of rise corresponding to increased acceleration. During shaking shearing of the bubble can be seen, which looks to be a combination of simple shear and contraction and may be related to fluid movement in the tank.

7. Discussion

The aim of this project set out to examine the effects of shaking on gas bubbles within viscoelastic fluids as an analogue for magmatic systems in earthquakes. The results of the experiments have answered the first three bullet points below. These results have been critically discussed in this chapter and several theories answering the last two points have been put forward.

- How is bubble behaviour affected during shaking in viscoelastic fluids? How is rise rate and shape affected?
- What effect do system parameters have on bubble behaviour during shaking?
    - Viscosity (Pa s)
    - Bubble size (m)
- What effect do shaking parameters have on bubble behaviour?
    - Displacement (mm) and frequency of shaking (Hz)
    - Acceleration of shaking (g) as a function of displacement and frequency where $g = 9.81$ m s^{-2} (Bueche, 1970).
    - Duration of shaking (seconds)
- What is the mechanism for accelerated rate of rise of a bubble during shaking?
- What are the implications of shaking bubble behaviour for natural geological systems?

The results from the experiments show that bubbles do show increased rise rate during shaking. Simply applied, a bubble can rise higher in the volcanic system during shaking. This has implications for triggering volcanic activity following earthquakes, through advective overpressure in closed systems and for outgassing in open systems. The height to which a bubble rises is important for both these processes and parts of the discussion will focus on height, h, risen in the discussion. When considering advective overpressure the formula takes height to which the bubble rises into account (Sahagian & Proussevitch, 1992; Pyle & Pyle, 1995). Details for advective over pressure have been given in Section 3.7.3 but will be revisited in the Implications section. The height to which a bubble is able to rise may also determine whether outgassing occurs. I will also postulate several mechanisms for increased rise rate of bubble during connected to the bubble shear observed and the known fluid rheology.

7.1 Effects of system parameters on bubble behaviour

Results of the experiments show that bubble size, viscosity, and duration of shaking do not have a direct effect on the change in rise rate of a bubble. But, they do control the height to which a bubble will rise in a given time, which has important implications for outgassing and advective overpressure. The larger the bubble the more buoyant it is compared to the surrounding liquid and the faster it will rise (Baz-Rodríguez et al., 2012), Similarly, lower viscosity fluids allow bubbles to rise faster than the same bubble in a higher viscosity fluid, as demonstrated in my experiments. Therefore, in a lower viscosity fluid a bubble may travel to a greater height, *h*.

The height, *h*, to which a bubble will travel in a given time, controls the increase in pressure through advective overpressure as well as outgassing. In a less viscous magma bubbles are able to rise, and possibly escape, more easily. Larger bubbles will rise faster and so the same applies to them. Systems of lower viscosities or those containing larger bubbles will therefore be more affected by outgassing or advective overpressure. This is not necessarily connected to shaking but it is important to note for understanding which systems may be more susceptible to the effects of shaking.

Duration of shaking does not correlate with the amount which the bubble rise rate increases but it does affect the height to which the bubble travels. The longer the duration of shaking, the higher the bubble will travel during the period where bubble rise is elevated. Increased rate of bubble rate occurs only while shaking occurs, as seen in the experiments. Therefore, the time for which a bubbles rise rate will increase is directly linked to how long it is shaken for. Systems which experience longer durations of shaking will be more affected (Trifunac & Brady 1975). This may be due to long duration earthquakes or due to the cumulative effects of multiple earthquakes.

7.2 Effects of shaking parameters on bubble behaviour

The shaking parameters displacement, frequency, and acceleration are interrelated given that;

$$a=-(2\pi f)^2 x \text{ (Lang, 2009)}$$

Where a is acceleration in ms^{-2}, f is frequency in Hz, and x is displacement from the central point. However, only acceleration showed a positive correlation with increased rates of bubble rise. Experiments with higher rates of increased rise came from both short and long

displacement experiments but were associated with relatively higher frequencies. This is due to acceleration being a product of both displacement and frequency (Wald et al., 1999).

Higher accelerations cause a greater increase in bubble rise rate. This indicates that volcanoes or geothermal systems which are subject to earthquakes producing higher accelerations, or PGA, will be more affected. These will likely undergo heightened bubble migration. This means that in a closed system advective overpressure will increase more as the height, *h*, attained will be greater (Pyle & Pyle, 1995; Sahagian & Proussevitch, 1992). And bubbles which travel faster and further in an open system are more likely to result in increased outgassing.

7.2.1 Bubble shear

The increased rise rate due to acceleration is believed to be connected to the bubble shear seen in the experiments. Bubble shear is defined by the capillary number, the ratio of those stresses (Rust et al., 2003). Bubble shear occurs as shear stresses acts upon the bubble, as a result of the effects of viscosity and velocity, which overcome stress associated with surface tension forces (Roman & Cashman, 2006; Rust et al., 2003). High shear rates tend to be associated with higher levels of bubble deformation (Rust et al., 2003). Studies concerning the capillary number of magmatic bubbles have focussed on magmatic and lava movement during flow and emplacement (Taddeucci et al. 2006; Rust et al. 2003) as opposed to oscillations driven by shaking.

In Figure 9, three possible bubble deformation end members have been presented (Segal, 2002). Figure 9a shows pure shear shape change of the bubble, but no volume change. As gas is compressible but the fluid is incompressible (Obermeier, 2015) the end member of pure shear is unlikely (Cihan & Corapcioglu, 2008). Similar bubble morphology changes have been seen in decompression or multiple bubble experiments and they are typically associated with volume changes as the bubble volume expands (Fig. 9b). (Taddeucci et al., 2006; L'Heureux, 2009). Figure 9b shows a volume change, or pumping (Fyrillas & Szeri, 1994), of the bubble similar to that which has been associated with rectified diffusion. The bubble undergoes expansion and contraction associated with diffusion of volatiles into the gas phase, theoretically resulting in a pressure increase (Ichihara & Brodsky, 2006; Plesset & Prosperetti, 1977; Fyrillas & Szeri, 1994). Figure 9c shows the bubble moving as simple shear, with no volume change.

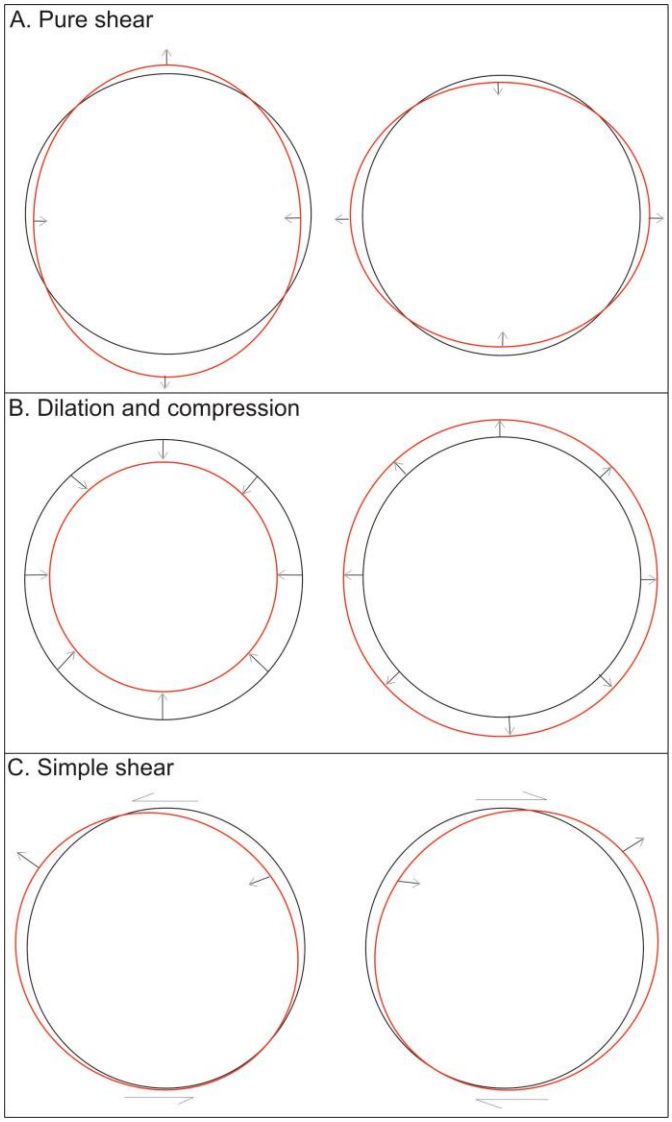

Figure 9. Image gives the end members of bubble morphology changes possible during shaking. Pure shear, dilation and compression, and simple shear.

When compared to the bubble overlay, (Fig. 10), it appears that the bubble moves in predominately a simple shear manner. Shear occurs in the direction opposite to shaking, acted upon by the relative fluid velocity within the tank (Segal, 2002). The silicon oil used for these experiments was incompressible. The bubbles in the experiments were made by injecting air, which is compressible. During shaking, the bubbles may compress and shear slightly due to being in an incompressible liquid and being acted upon by acceleration, *g* (Lang, 2009). The capillary number ratio shifts so that the force of surface tension is overcome, allowing for bubble deform, or shear (Roman & Cashman, 2006; Rust et al., 2003). A fluid velocity gradient develops in the tank during acceleration and this drives a relative shear on the bubble (Rust et al. 2003). The incompressible fluid and the force, *g*, causes a shape change and simple shearing. The smaller amount of blue in Figure 10 compared to red indicates that there

is also a small contraction in volume but the resolution used was not fine enough to determine this accurately. Further work at higher resolutions and high-speed filming is suggested to determine of this phenomena has occurred.

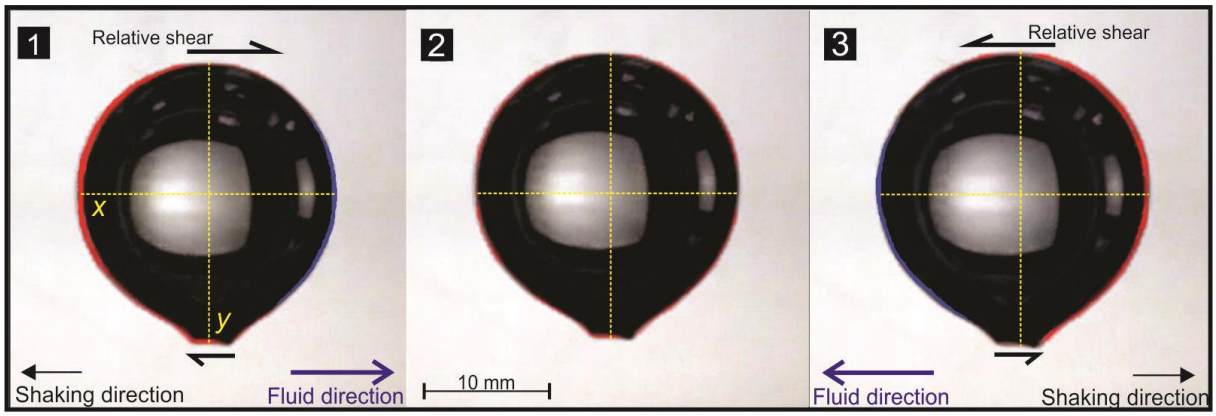

Figure 10. The figure from results has been used again here to show bubble shear related to discussion and implications for the mechanisms of increased rise rate.

7.2.2 Viscosity dependency on shaking parameters

Another possibility is that the shear stress induced by shaking was sufficient to drive shear thinning in the in the non-Newtonian silicone oils, causing viscosity to decrease (Schapery, 1969; Obermeier, 2015; Llewellin & Manga, 2005). High shear strain rates are associated with higher acceleration of shaking (Lang, 2009). Given this, the decrease of viscosity associated with that may be the mechanism for increased rates of bubble rise. The silicon fluid used has a viscosity dependant on shear strain rate, particularly at higher shear strain rates (Obermeier, 2015; Parmigiani et al., 2016; Lyon, 2016; Ichihara et al., 2004). Using the velocity of shaking, derived from the displacement and frequency, and the s-wave propagation velocity in silicone oil the effects of shaking on the viscosity have been investigated. The s-wave propagation velocity of the silicone oil with a viscosity of $\geq 10^5$ Pa s is 39±24 m/s (Ichihara et al., 2004). Velocity (m/s) has been calculated using $V=\pi FD$, where F (Hz) is the frequency and D (m) is the total distance travelled (Lang, 2009). The imposed velocity is then divided by the s-wave propagation velocity giving the strain. Shear strain rate is then calculated by; shear strain rate [1/s] = $(2\pi F)$ multiplied by strain (Lang, 2009). The results of this have been given in Table 6.

Table 6. Calculated values used for determining shear strain rate viscosity dependency.

Parameter	E5	E6	E7	E8	E9	E10	E11
Velocity (m/s)	0.06283	0.18850	0.37699	0.75398	0.80425	0.25133	0.80425
Strain	0.001611	0.004833	0.009666	0.019333	0.020622	0.006444	0.020622
Shear strain rate	0.010123	0.091104	0.060736	0.242944	0.207312	0.161963	0.207312

If these results are plotted onto the viscosity dependency (Fig. 11) some assumptions can be made about the viscosity during shaking due to shear strain rates. I have plotted on the highest shear strain rate, 0.24 [1/s]. The viscosities used for the experiments were 2,000,000 mP s, 10,000,000 mPa s 30,000,000 mPa s. The viscosities in Figure 11 only reach as high as 1,000,000 mPa s as rheological methods are unable to produce data for higher viscosities.

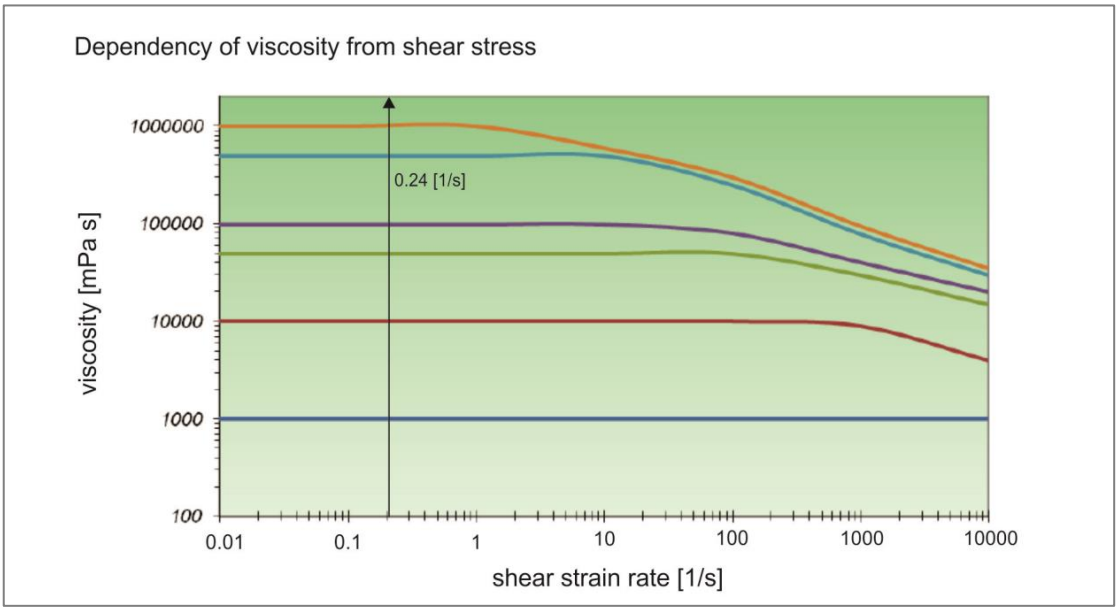

Figure 11. Dependence of viscosity based on shear strain rate. A shear strain rate of 0.24 1/s has been plotted on as it is the highest experienced during experiments. The rheology figure given by Obermeier gives viscosity in mPa s, not Pa s.

The shear rate dependence of viscosity is difficult to determine experimentally using rheometers (Lejeune et al., 1999; Divoux et al., 2011; Giordano et al., 2008; Bair & Winer, 1992). Viscosity dependence above 1,000,000 mPa s could not be determined using typical rheological methods and must be extorapolated (Giordano et al., 2008; Bair & Winer, 1992). Other methods may be able to produce this data but they were not available within the scope of this project. The data given by Obermeier in Figure 9 only gives the dependency up to 1,000,000 mPa s, or 1,000 Pa s. They were unable to produce viscosity dependency data for viscosities higher than this but state that the higher the viscosity the sooner the viscosity will decrease (Dr. Thomas Wenzel, Obermeier, personal communication, February 23, 2017). If

the trends from Figure 10 continued into higher viscosities it is likely that the viscosities tested would have lowered during shaking with produced higher shear strain rates. It is difficult to say to what extent this occurred for the velocities and viscosities tested.

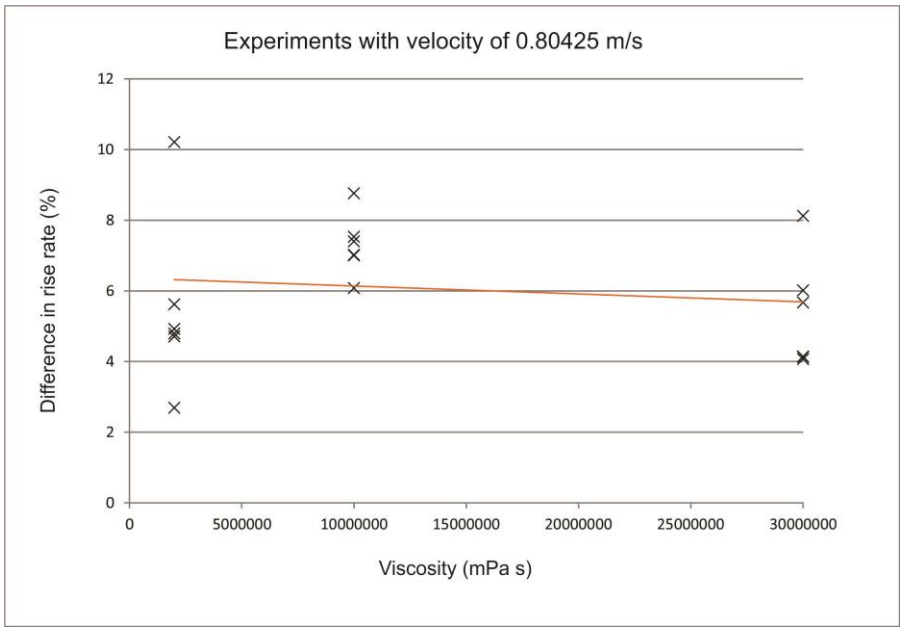

Figure 12. Bubble rise rate changes for experiments which experienced shear strain rates of 0.80425 1/s plotted against viscosity.

Experiments (Fig. 11), with the same velocity have been plotted against viscosity to see if there is a noticable trend in rise rate increase which could be explained through strain rate dependent viscosity changes. The experiments plotted represent those which had a velocity of 0.80425 m/s and a shear strain rate of 0.21 1/s. A linear trendline was fitted to the differences in rise rate. However, the correlation is very weak and for this reason I am hesistant to invoke the shear strain rate dependence of viscosity as the driving mechanism to explain the change in rise rate.

With finer resolution images it may be possible to connect the amount of bubble shear to the velocity and viscosity decrease. The decrease in viscosity due to the shear strain rate may be sufficient to facilitate the shear of the bubble seen in the experiments. At higher velocities, when viscosity is assumed to have decreased more significantly, bubbles may shear to a greater extent (Baz-Rodríguez et al., 2012). Further work in finer resolution is needed to determine the extent to which decreased viscosity affects bubble rise rate and bubble shear amount.

7.2.3 Net force lift as a mechanism for increased rise rate

Another possible rise mechanism is that lateral fluid flow across a sheared bubble causes a lift force, increasing the rise rate (Nakayama et al., 1998). Lift force is the force which acts upon an appropriately oriented asymmetric body due to fluid flowing past it. This is similar to how an airplane flies, with the wind acting upon the asymmetrical shape of the wing providing the lift. During shaking the bubble shear away from the direction of movement, causing the bubble to become asymmetrical. When the shaking direction changes the fluid flow direction will be reversed and the sheared bubble will be suitably oriented to generate lift (Fig. 12). The lift force may act on the bubble during the scenario pictured below, a period of lift will be generated until the bubble re-deform into the opposite sense of shear, and lift would not be generated until shaking direction again changes. Theoretically this may be a mechanism for increased rate of rise but further investigation necessitates delving further into the realm of fluid mechanics modelling.

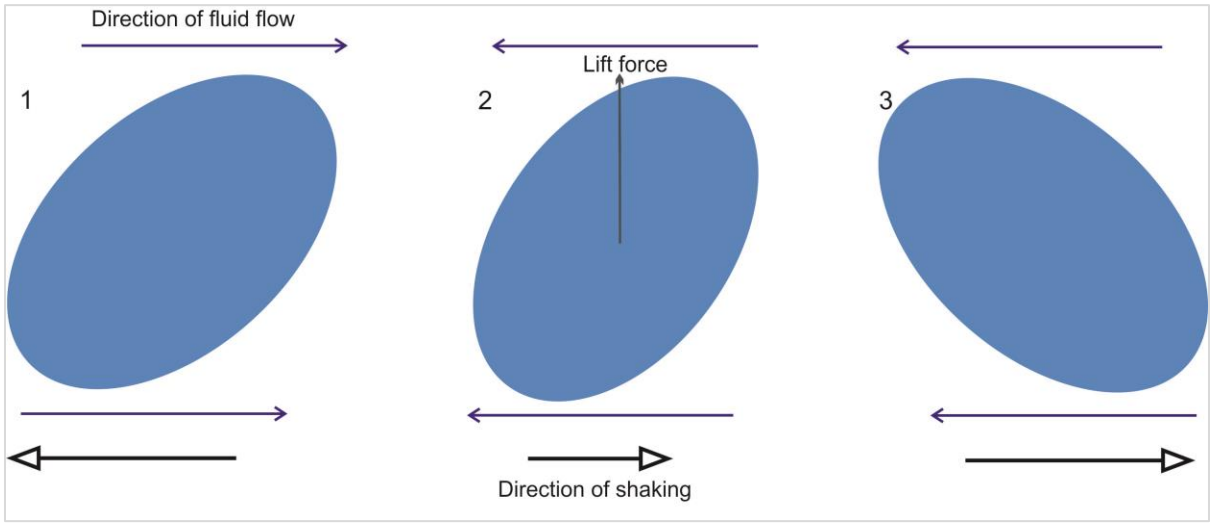

Figure 13. Lift force acts upon a sheared bubble as direction of shaking causes fluid flow in the opposite direction.

8. Implications

The results of this project have implications for volcanic activity triggered by earthquakes. Upwards migration of bubbles causes outgassing in open systems and may lead to pressure increases, through advective overpressure, in closed systems. Bubbles which migrate faster due to shaking may cause increases in both of these processes which may lead to triggered activity.

8.1 A simplified laboratory system

In a simplified laboratory system the effects of advective overpressure can be seen numerically estimated (Pyle & Pyle, 1995; Sahagian & Proussevitch, 1992; Manga & Brodsky, 2006). By comparing the pressure increase due to a non-shaking bubble to a shaking bubble the effects of shaking can be modelled. The calculation is based on a bubble rising to a height in a fully sealed cylinder which is fully filled with a fluid. To calculate the change in pressure due to advective over pressure we use the following formula:

$$\Delta Pmax = \rho g \Delta H \text{ (Manga \& Brodsky, 2006)}$$

Where ΔP is the pressure change due to bubble rise, ρ is fluid density of 0.00097 kg/m³ (Obermeier, 2015), g is acceleration due to gravity 9.8 m/s/s, and Δh is height which the bubble ascends. For a viscosity of 2,000 Pa s and bubble size of 25 mms it has a still rise rate of 1.39×10^{-2} 0.0139 m/minute. The change due to advective overpressure is as follows;

$$(9.7 \times 10^{-4} \text{ kg/m}^3)(9.8 \text{ m/s/s})(1.39 \times 10^{-2} \text{ m}) = 1.3213 \times 10^{-4} \text{ kg/(m·s}^2)$$

In a shaking experiment for a 25 mm bubble in 2,000 Pa s which lasted 60 seconds (I have chosen to use results from parameter E11) bubble velocity increased by 4.92 %. Thus, in the same time the bubble will have travelled 4.92% further than 0.0139, rising to 0.0146 m/minute. Using the height gained due to shaking the following is true of the advective overpressure change;

$$(9.7 \times 10^{-4} \text{ kg/m}^3)(9.8 \text{ m/s/s})(1.46 \times 10^{-2} \text{ m}) = 1.3879 \times 10^{-4} \text{ kg/(m·s}^2)$$

In a shaking scenario the pressure has risen 6.6542×10^{-6} kg/(m·s²) more than the non-shaking scenario due to the height change over the same period of time. This is calculated in Pascals by multiplying it by g, giving us a pressure change of 6.5255×10^{-5} Pa.

Pressure was measured during the experiments using a Keller Highly Precise Pressure Transmitter, series PR33X / 80794, but no measurable changes were observed. However, the very small rise in pressure calculated above is below the detection limit of the pressure gauges used in the experiment. The pressure sensor can measure as low as 0.8 bar, which is equal to 100,000 Pa. The calculated change due to advective overpressure is far below 80,000 Pa and is therefore below the detectable limit.

8.2 Implications and applications for natural systems

As outlined in the beginning of this thesis, there are many triggering methods which have been hypothesized. These may be static, dynamic, or a combination of both (Manga & Brodsky, 2006). Static stress changes have been well researched with regards to stress fields changing on adjacent faults and around volcanic edifices (e.g. Hill, Pollitz & Newhall, 2002; King, Stein & Lin, 1994; Walter, 2007). Dynamic triggers include; advective overpressure, cavitation, rectified diffusion, bubble detachment, and coalescence, have also been proposed. These can affect both open (Namiki et al., 2016) and sealed magmatic systems (Manga & Brodsky, 2006) as well as mud volcanoes (Manga et al., 2009; Davies et al., 2008) and geothermal systems (Linde et al., 1994).

8.2.1 Outgassing volcanic, magmatic, and geothermal systems

Increased rates of outgassing at volcanoes (Walter et al., 2009; Cigolini et al., 2007), mud volcanoes (Davies et al., 2008; Manga et al., 2009), and geothermal systems (Crews & Cooper, 2014) are known to have occurred following earthquakes. Outgassing of these systems may be linked to the results of this project. As bubbles travel faster during shaking, and may be shaken loose and mobilised, they can then escape as outgassing volatiles.

Outgassing has been associated with seismicity at the volcano Merapi in Indonesia (Jousset et al. 2013). A study in 2013 showed that during seismicity, both tectonic and volcano-tectonic, Merapi increased outgassing from monitored vents. They postulate that the volcanic seismicity may have been caused by the release of gas but that it is also likely that the gas release was triggered by the seismicity. The seismicity in this study preceded a large eruption at Merapi, evidence that dynamic triggering may have been involved in the eruptions.

Similar reactions to earthquakes have also been detected at Mt Etna, in Italy (Carbone et al. 2009; Walter et al. 2009). Gravity changes, due to mass relocation, have been detected during

local earthquakes at Mt Etna (Carbone et al. 2009). Several mechanisms may have triggered the gravity changes including bubble and crystal mass redistribution. Bubbles being shaken loose or rising faster may have been part of the mass redistribution. Monitoring micro-gravity changes, in addition to gas monitoring, may be another way to detect bubble migration related to seismicity for future studies.

In September 2002 several earthquakes were followed by volcanic activity at Mount Etna, Stromboli Island, and anomalous outgassing near Panarea Island (Walter et al., 2009). This increased activity has been linked to static and dynamic stress changes caused by the tectonic activity. The exact trigger which caused these phenomena is unknown but may be linked to bubbles rising faster during shaking. Bubbles may also have been shaken loose from crystals and begin to rise or be activated due to crystal mush overturn.

If shaking causes increased rates of outgassing in unsealed systems, allowing the system to flush its pressure (Yoshimura & Nakamura, 2008), it may lessen the chance of an eruption, instead of increase it (Namiki & Manga, 2006). If this occurs it is more likely to occur in basaltic systems, than the more viscous end-members. This is because bubbles rise more freely in less viscous fluids (Parmigiani et al., 2016) and will rise and escape. If the bubble is not able to escape due to viscosity, the magma will become more pressurized instead of outgassing through advective overpressure as discussed above (Sahagian & Proussevitch, 1992) which may lead to eruption. The relationship between volcanoes and earthquakes would benefit greatly from further research looking into outgassing behaviour following earthquakes.

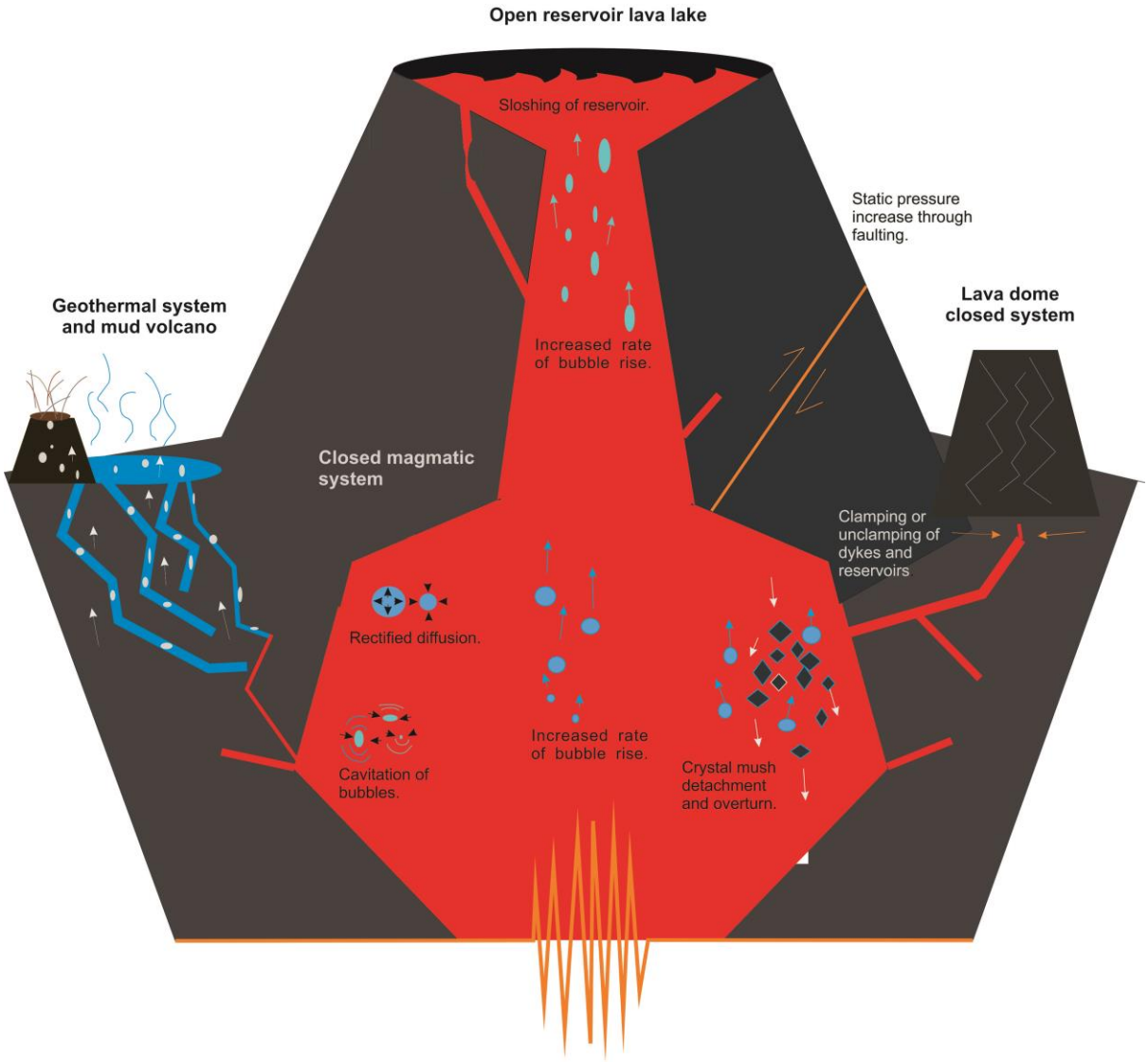

Figure 14. Volcanic and magmatic system with possible triggering mechanisms from earthquakes.

8.2.2 Advective overpressure

Advective overpressure has been proposed as a possible mechanism for advancing volcanic eruptions following earthquakes (e.g. Manga & Brodsky, 2006; Sahagian & Proussevitch, 1992; Steinberg, Steinberg & Merzhanov, 1989; Watt, Pyle & Mather, 2009). It can occurs in closed systems where pressure can increase (Fig. 14), in any part of the reservoir and in geothermal features. However, the formula used to calculate the advective overpressure in laboratory experiments is not applicable for large-scale natural systems (Bagdassarov, 1994; Pyle & Pyle, 1995). A more in depth analysis and application of the results from my experiments is beyond the scope of this project.

Sahagian and Proussevitch (1992) applied the advective overpressure calculation to both a laboratory experiment and a simplified magma chamber. Their calculation showed that a bubble rising in a homogenous magma chamber would cause a significant pressure increase. However, they point out that the conditions necessary for this are unlikely to be fully met in a natural system. The volcano may not be fully sealed allowing leakage and deformation may occur. They point out that this mechanism is likely a supplement to crystallization or magmatic recharge processes (Sahagian & Proussevitch, 1992).

Bagdassarov (1994) and Pyle and Pyle (1995) are less positive about the application of the advective overpressure calculations to magmatic systems. Pyle and Pyle (1995) ran similar models to Sahagian and Proussevitch (1992) but concluded that advective overpressure would mainly affect magmas containing large bubbles and that CO_2 dominated systems would be more affected due to the effects of diffusion. Bagdassarov (1994) also points out the need to take compressibility and volumes of both the gas and the fluid into account. Otherwise the application to a large-scale system is impossible to carry out accurately.

While the effects of advective overpressure cannot be applied numerically in the scope of this paper the simple laboratory tests do suggest several interesting things. My results show that any effects of advective over pressure will be increased with shaking which causes bubbles to rise faster. In addition, bubble size controls the rise velocity, based on Stoke's Law (Talaia, 2007; Merle, 2015). Smaller bubbles will rise to a lesser height during the same time frame as larger bubbles (Talaia, 2007), rendering their effect on increased pressure less. Bubbles which have a faster rise velocity or rise higher will have a larger effect on advective overpressure increases. Viscosity has a similar effect, as it controls bubble rise velocity (Llewellin et al., 2016). Therefore, systems which contain bubbles which may naturally rise faster may be more affected with regards to advective overpressure (Sahagian & Proussevitch, 1992).

The experimental results show that bubbles only appear to be affected during shaking, and do not show lingering effects (Fig. 5). From this it may be concluded that a bubble in a magma chamber will likewise only increase its rise velocity during shaking. Earthquake duration, or more accurately, the duration of which seismic waves affect the bubbles in the magma chamber will then be a control on how much advective overpressure is affected. Bubbles which are subject to longer durations of shaking (Salmon et al., 1992) which increases their rise rate will cause a higher pressure increase. Similarly, a magma chamber which is subject

to more earthquakes, or an earthquake and aftershock swarm (Hill, 1977; Roman & Cashman, 2006; Ardeleanu et al., 2012) will be more affected due to cumulative effects.

8.2.3 Cavitation, rectified diffusion, crystal detachment and crystal mush overturn, and bubble coalescence

The increase rate of rise seen in my experiments may affect other dynamic triggering mechanisms which have been discussed preciously. Other suggested triggers; crystal detachment and overturn, coalescence, cavitation, advective overpressure, rectified diffusion, may be affected by increased rate of bubble rise (Fig. 14). The results of this thesis may be loosely applied to these processes from a theoretical viewpoint.

If bubbles are shaken loose from crystals they have been attached to they are then free to rise (Boudreau, 2016). This process may also lead to crystal mush overturn (Namiki et al., 2016; Parmigiani et al., 2016; Manga & Brodsky, 2006). Crystal mush can impede the rise and migration of bubbles within a system (Boudreau, 2016; Parmigiani et al., 2016). When shaken loose or the crystal mush is displaced they are then free to rise and pressurize the system. The shaking may lead to bubbles interacting with one another, causing coalescence. The bubble, now larger, will rise faster in the system (Baz-Rodríguez et al., 2012) which may affect the pressure (Pyle & Pyle, 1995) and interaction with other bubbles and crystal matter. Experiments which look into bubble coalescence may be useful for this field of study.

At no point during the experiments did bubbles collapse, leading to cavitation. While the experiments were pressurized it is expected that the pressure was not high enough to cause the compression of the gas (Plesset & Prosperetti, 1977) to facilitate this. While this process has been highly research for industrial purposes (Kedrinskii et al., 2005; Ichihara et al., 2004) it has yet to be successfully applied to geologic processes.

The results of the experiments did not show volume changes of the bubbles, although this may be due to resolution. If detected, volume changes could indicate that processes involved with rectified diffusion may occur. The relative amounts of red and blue in Fig. 6 show that compression and expansion oscillations associated with rectified diffusion may have occurred (Ilinskii et al., 2008; Ichihara & Brodsky, 2006). However, the pressure dependent gas diffusion between air and silicone oils is not suitable to examine this process in detail. I suggest further work to look at volume changes of bubble during shaking and the extent to which this may affect geologic systems.

9. Conclusions

The results of this project have shown that shaking does have an effect on bubble rise rate and morphology in viscoelastic fluids. Rise rate was shown to increase from 1.91 to 13.33 %, with an average of 6.20 %. Bubble shape changes occur during shaking with a simple shear component and a possible compression component. This shear component is likely to contribute to the increased rise rate. The results of this project may also have interesting implications for industrial applications involving removal of bubbles from fluids.

System parameters, bubble size and viscosity of the fluid, do not have an overall effect on the percentage by which bubble rise rate increases. However, they are important when considering advective overpressure calculations and outgassing potential as they control the height to which a bubble will travel. Duration of shaking has a similar effect, as the longer shaking lasts the longer the period of time which rise rate is increased.

Shaking experiments with higher acceleration are associated with a greater increase in the rise rates of bubbles. This may be related to a decrease in viscosity due to shear strain rate but the results do not show a clear correlation with increases and viscosity. The partial rheometry data provided by Obermeier indicate that a viscosity decrease due to the shear strain rate induced by shaking is also likely to contribute to the increased rise rate. I conclude that high accelerations in our non-Newtonian fluids result in a greater maximum value and range of shear strain and a capillary number allowing bubble deformation. I have also suggested the possibility that lift generated when a sheared bubble is subject to lateral fluid flow or an appropriate orientation, leading to increased rise rate. Lift associated with sheared bubbles and combined with lowered viscosity due to the shear thinning are a likely mechanisms for increased rate of bubble rise.

When the results of the experiments were applied to a simple advective overpressure model it can be demonstrated that shaking causes an increase compared to a non-shaking scenario. When modelling a simplified magma chamber with advective overpressure a non-shaking bubble rising 1 cm caused pressure to rise by 2.00×10^{-5} % while the shaking bubble caused a pressure increase of 2.12×10^{-5} %.

Shaking does cause an increase in bubble rise rate, and this in turn increases advective overpressure when compared to non-shaking events. As acceleration, appears to drive the increasing rate of rise, it is likely that magmatic systems near the earthquake source will be

more affected, as PGA is likely to be higher (Cramer & Darragh, 1994). However, the amount to which this affects a magma chamber pressure is difficult to assess. My data does clearly provide a robust explanation for indicators of increased outgassing (Carbone et al., 2009; Jousset et al., 2013) measured at active volcanoes. However, this effect must be considered in combination with static stress changes and other dynamic stress changes in order to make predictive inferences between volcanic activity following earthquakes (Manga & Brodsky, 2006).

10. Acknowledgements

I offer my sincerest thanks and gratitude to my Ben Kennedy, for giving me this opportunity to take on this project. To all of the amazing people who offered the help and encouragement which got me through this! And an enormous thanks to Paul Ashwell and Alison Jolly for your support while I was working in Germany. Your messages helped me more than you can possibly imagine!

10. References

Ardeleanu, L., Grecu, B. & Raileanu, V., 2012. Peak ground acceleration, velocity and displacement from moderate magnitude undercrustal earthquakes of Vrancea region. *Romanian Reports in Physics*, 64(2), pp.555–570.

Bagdassarov, N., 1994. Pressure and volume changes in magmatic systems due to the vertical displacement of compressible materials. *Journal of Volcanology and Geothermal Research*, 63, pp.95–100.

Bair, S. & Winer, W. O., 1992. The High Pressure High Shear Stress Rheology of Liquid Lubricants. *Journal of Tribology*, 114(January), p.1.

Baker, D. R., Freda, C., Brooker, R. A. Scarlato, P. 2005. Volatile diffusion in silicate melts and its effects on melt inclusions. *Annals of Geophysics*, 48(4–5), pp.699–717.

Barrientos, S. E., 1994. Large thrust earthquakes and volcanic eruptions. *Pure and Applied Geophysics PAGEOPH*, 142(1), pp.225–237.

Baz-Rodríguez, S., Aguilar-Corona, A. & Soria, A., 2012. Rising velocity for single bubbles in pure liquids. *Revista Mexicana de Ingeniería Química*, 11(2), pp.269–278.

Bebbington, M. S. & Marzocchi, W., 2011. Stochastic models for earthquake triggering of volcanic eruptions. *Journal of Geophysical Research*, 116(B5), pp.1–16.

Beckett, F. M., Burton, M., Mader, H. M., Phillips, J. C., Polacci, M. Rust, A. C., Witham, F., 2014. Conduit convection driving persistent degassing at basaltic volcanoes. *Journal of Volcanology and Geothermal Research*, 283, pp.19–35.

Del Bello, E. Llewellin, E. W.,Taddeucci, J., Scarlato, P., Lane, S. J., 2012. An analytical model for gas overpressure in slug-driven explosions: Insights into Strombolian volcanic eruptions. *Journal of Geophysical Research: Solid Earth*, 117(2).

Blake, J. R. & Gibson, D. C., 1987. Cavitation bubbles near boundaries. *Annual Review of Fluid Mechanics*, 19, pp.99–123.

Bonali, F. L. Tibaldi, A., Corazzato, C., Tormey, D.R., Lara, L.E., 2012. Quantifying the effect of large earthquakes in promoting eruptions due to stress changes on magma pathway: The Chile case. *Tectonophysics*, 583, pp.54–67.

Boudreau, A., 2016. Bubble migration in a compacting crystal-liquid mush. *Contributions to Mineralogy and Petrology*, 171(4), pp.1–17.

Bueche, F., 1970. Introduction to Physics for Scientists and Engineers. *American Journal of Physics*, 38(2), p.274. Available at: http://scitation.aip.org/content/aapt/journal/ajp/38/2/10.1119/1.1976308 [Accessed December 12, 2016].

Candela, T., Brodsky, E., Marone, C., Elsworth, D., 2014. Laboratory evidence for particle mobilization as a mechanism for permeability enhancement via dynamic stressing. *Earth and Planetary Science Letters*, 392, pp.279–291. Available at: http://dx.doi.org/10.1016/j.epsl.2014.02.025.

Carbone, D., Jousset, P. & Musumeci, C., 2009. Gravity "steps" at Mt. Etna volcano (Italy): Instrumental effects or evidences of earthquake-triggered magma density changes? *Geophysical Research Letters*, 36(2), pp.1–6.

Chen, B. F. & Nokes, R., 2005. Time-independent finite difference analysis of fully non-linear and viscous fluid sloshing in a rectangular tank. *Journal of Computational Physics*, 209(1), pp.47–81.

Chhabra, R .P., 2006. Non-Newtonian Fluid Behavior. In *Bubbles, Drops, and Particles in Non-Newtonian Fluids, Second Edition*. Boca Raton, Florida: CRC Raylor & Francis, pp. 9–47.

Cigolini, C., Laiolo, M. & Coppola, D., 2007. Earthquake-volcano interactions detected from radon degassing at Stromboli (Italy). *Earth and Planetary Science Letters*, 257(3–4), pp.511–525.

Cihan, A., Corapcioglu, M. Y., 2008. Effect of compressibility on the rise velocity of an air bubble in porous media. *Water Resources Research*, 44(4), p.n/a-n/a. Available at: http://doi.wiley.com/10.1029/2006WR005415 [Accessed February 23, 2017].

Le Corvec, N., Menand, T. & Lindsay, J., 2013. Interaction of ascending magma with pre-existing crustal fractures in monogenetic basaltic volcanism: an experimental approach. *Journal of Geophysical Research: Solid Earth*, 118(3), pp.968–984. Available at: http://doi.wiley.com/10.1002/jgrb.50142 [Accessed December 11, 2016].

Cramer, C. H. & Darragh, R. B., 1994. Peak accelerations from the 1992 Landers and Big Bear, California, earthquakes. *Bulletin of the Seismological Society of America*, 84(3), pp.589–595.

Crews, J. B. & Cooper, C. A., 2014. Experimental evidence for seismically initiated gas bubble nucleation and growth in groundwater as a mechanism for coseismic borehole water level rise and remotely triggered seismicity. *Journal of Geophysical Research B: Solid Earth*, 119, pp.1–13.

Cross, R., 2012. Elastic and viscous properties of Silly Putty. *American Journal of Physics*, 80(2012), p.870.

Davies, R. J. Brumm, M., Manga, M., Rubiandini, R., Swarbrick, R., Tingay, M., 2008. The East Java mud volcano (2006 to present): An earthquake or drilling trigger? *Earth and Planetary Science Letters*, 272(3–4), pp.627–638. Available at: http://dx.doi.org/10.1016/j.epsl.2008.05.029.

Dingwell, D. B., 2006. Transport Properties of Magmas : Diffusion and Rheology. *Elements*, 2(5), pp.281–286.

Dingwell, D. B. & Bagdassarov, N., 1993. Deformation of foamed rhyolites under internal and external stresses: an experimental investigation. *Bulletin of Volcanology*, 55, pp.147–154.

Divoux, T. Vidal, V., Ripepe, M., Géminard, J C., 2011. Influence of non-Newtonian rheology on magma degassing. *Geophysical Research Letters*, 38(May), pp.3–7.

Dzierma, Y. Thorwart, M., Rabbel, W., Siegmund, C., Comte, D., Bataille, K., Iglesia, P., Prezzi, C., 2012. Seismicity near the slip maximum of the 1960 Mw 9.5 Valdivia earthquake (Chile): Plate interface lock and reactivation of the subducted Valdivia Fracture Zone. *Journal of Geophysical Research*, 117(B6), p.B06312. Available at: http://doi.wiley.com/10.1029/2011JB008914.

Eggert, S. & Walter, T. R., 2009. Volcanic activity before and after large tectonic earthquakes: Observations and statistical significance. *Tectonophysics*, 471(1–2), pp.14–26. Available at: http://linkinghub.elsevier.com/retrieve/pii/S0040195108004757.

F. J. Spera, 2000. Physical properties of magma. In *Encyclopedia of Volcanoes*. pp. 338–339.

Frandsen, J. B., 2004. *Sloshing motions in excited tanks*,

Fujita, E., Kozono, T. & Ueda, H., 2013. Stress field change around the Mount Fuji volcano magma system caused by the Tohoku megathrust earthquake , Japan. *Bulletin of Volcanology*, 75(679).

Furbish, D. J., 1997. *Fluid Physics in Geology: An Introduction to Fluid Motions on Earth's Surface and Within Its Crust* First Edit., Oxford: Oxford University Press.

Fyrillas, M. M. & Szeri, A. J., 1994. Dissolution or growth of soluble spherical oscillating bubbles: the effect of surfactants. *Journal of Fluid Mechanics*, 289(1), p.381. Available at: http://www.journals.cambridge.org/abstract_S0022112094002806%5Cnhttp://www.journals.cambridge.org/abstract_S0022112095001340.

Galland, O. Holohan, E., van Wyk de Vries, B., Burchardt, S., 2015. Laboratory modelling of volcano plumbing systems: a review. *Advances in Volcanology*, (9).

Galland, O. Cobbold, P. R., de Bremond d'Ars, J., Hallot, E., 2007. Rise and emplacement of magma during horizontal shortening of the brittle crust: Insights from experimental modeling. *Journal of Geophysical Research*, 112(b6).

GeoSIG Ltd, 2009. GSK-166 Uniaxial Linear Shaking Table. *GS Shaker Leaflet*, 5.

Giordano, D., Russell, J. K. & Dingwell, D. B., 2008. *Viscosity of magmatic liquids: A model*,

Gualda, G. A. R. & Anderson, A. T., 2007. Magnetite scavenging and the buoyancy of bubbles in magmas. Part 1: Discovery of a pre-eruptive bubble in Bishop rhyolite. *Contributions to Mineralogy and Petrology*, 153(6), pp.733–742.

Gudmundsson, A. & Andrew, R. E. B., 2007. Mechanical interaction between active volcanoes in Iceland. *Geophysical Research Letters*, 34(April), pp.1–5.

Gurenko, A. A. Belousov, A. B., Trumbull, R. B., Sobolev, A. V.., 2005. Explosive basaltic volcanism of the Chikurachki Volcano (Kurile arc, Russia): Insights on pre-eruptive magmatic conditions and volatile budget revealed from phenocryst-hosted melt inclusions and groundmass glasses. *Journal of Volcanology and Geothermal Research*, 147(3–4), pp.203–232.

Hakala, T., Suomalainen, J. & Peltoniemi, J.I., 2010. Acquisition of Bidirectional Reflectance Factor Dataset Using a Micro Unmanned Aerial Vehicle and a Consumer Camera. *Remote*

Sensing, 2(3), p.819. Available at: http://www.mdpi.com/2072-4292/2/3/819.

Heap, M. J. Xu, T., Kushnir, A. R. L., Kennedy, B. M., Chen, C., 2015. Fracture of magma containing overpressurised pores. *Journal of Volcanology and Geothermal Research*, 301, pp.180–190. Available at: http://linkinghub.elsevier.com/retrieve/pii/S0377027315001687.

Hill, D. P., 1977. A model for earthquake swarms. *Journal of Geophysical Research*, 82(8), pp.1347–1352. Available at: http://doi.wiley.com/10.1029/JB082i008p01347 [Accessed February 19, 2017].

Hill, D. P., Pollitz, F. & Newhall, C., 2002. Earthquake–Volcano Interactions. *Physics Today*, 55(11), pp.41–47. Available at: http://scitation.aip.org/content/aip/magazine/physicstoday/article/55/11/10.1063/1.1535006.

Holtz, F. Scaillet, B., Behrens, H., Schulze, F., Pichavant, M., 1996. Water content of felsic melts: application to the rheological properties of granitic magmas. *GSA Special Papers*, 315, pp.57–64.

Housener, G. W., 1963. The dynamic behavior of water tanks. *Bulletin of the Seismological Society of Amerrica*, 53(2), pp.381–387.

Housner, G. W., 1957. Dynamic pressures on accelerated fluid containers. *Bulletin of the Seismological Society of America*, 47(1), pp.15–35. Available at: http://www.bssaonline.org/cgi/content/abstract/47/1/15.

Huppert, H. E. & Woods, A. W., 2002. The role of volatiles in magma chamber dynamics. *Nature*, 48(1988), pp.493–496.

Ichihara, M. Ohkunitani, H., Ida, Y., Kameda, M., 2004. Dynamics of bubble oscillation and wave propagation in viscoelastic liquids. *Journal of Volcanology and Geothermal Research*, 129(1–3), pp.37–60.

Ichihara, M. & Brodsky, E. E., 2006. A limit on the effect of rectified diffusion in volcanic systems. *Geophysical Research Letters*, 33(2), pp.1–5.

Ilinskii, Y., Wilson, P. S. & Hamilton, M. F., 2008. Bubble growth by rectified diffusion at high gas supersaturation levels. *The Journal of the Acoustical Society of America*, 124(4), pp.1950–1955.

Jousset, P. Sule, Diningrat, W., Syahbana, D., Gassner, A., Akbar, F., Guichard, S., Schuck, N., Ryannugroho, R., Hendryana, A., Kusnadi, Y., Nugraha, A., Muksin, U., Jaya, M., Pratomo, B., Erbas, K., Bruhn, D., 2015. Seismic tomography and dynamics of geothermal and natural hydrothermal systems in the south of Bandung , Indonesia. *World Geothermal Congress 2015*, 17(April), p.14343.

Jousset, P.., Budi-Santoso, A., Jolly, A., Boichu, M., Surono, Dwiyono, S., Sumarti, S., Hidayati, S., Thierry, P., 2013. Signs of magma ascent in LP and VLP seismic events and link to degassing: An example from the 2010 explosive eruption at Merapi volcano, Indonesia. *Journal of Volcanology and Geothermal Research*, 261, pp.171–192. Available at: http://dx.doi.org/10.1016/j.jvolgeores.2013.03.014.

Kedrinskii, V. Makarov, A., Stebnovskii, S., Takayama, K., 2005. Explosive Eruption of Volcanoes: Some Approaches to Simulation. *Combustion, Explosion, and Shock Waves*, 41(6), pp.777–784. Available at: http://dx.doi.org/10.1007/s10573-005-0086-z.

Kedrinskiy, V., 2008. Hydrodynamic aspects of explosive eruptions of volcanoes: simulation problems. *Shock Waves*, 18(6), pp.451–464. Available at: http://link.springer.com/10.1007/s00193-008-0181-7.

King, G. C. P., Stein, S. & Lin, J., 1994. Static stress changes and the triggering of earthquakes. *Bulletin of the Seismological Society of America*, 84(3), pp.935–953.

Klügel, A. Walter, T. R., Schwarz, S., Geldmacher, J., 2005. Gravitational spreading causes en-echelon diking along a rift zone of Madeira Archipelago: an experimental approach and implications for magma transport. *Bulletin of Volcanology*, 68(1), p.37. Available at: http://dx.doi.org/10.1007/s00445-005-0418-6.

Kurahashi, S. & Irikura, K., 2011. Source model for generating strong ground motions during the 2011 off the pacific coast of tohoku earthquake. *Earth, Planets and Space*, 63(7), pp.571–576.

L'Heureux, I., 2009. Volatile bubble growth in a decompressing magmatic system: A many-bubble model. *Journal of Geophysical Research: Solid Earth*, 114(12), pp.1–9.

Lang, H., 2009. *Head first physics: a learner's companion to mechanics and practical physics* 1st Editio., O'Reilly Media.

Lara, L. E., Naranjo, J. A. & Moreno, H., 2004. Rhyodacitic fissure eruption in Southern Andes (Cordon Caulle; 40.5S) after the 1960 (Mw:9.5) Chilean earthquake: A structural interpretation. *Journal of Volcanology and Geothermal Research*, 138(1–2), pp.127–138.

Lejeune, A. M., Bottinga, Y., Trull, T. W., Richet, P., 1999. Rheology of bubble-bearing magmas. *Earth and Planetary Science Letters*, 166, pp.71–84.

Li, K., 2008. The image stabilizer plugin for ImageJ.

Linde, A. T., Sacks, I. S., Johnston, M. J. S., Hillt, D. P., Bilham, R. G.., 1994. Increased pressure from rising bubbles as a mechanism for remotely triggered seismicity. *Nature*, 371, pp.408–410. Available at: http://www.nature.com/nature/journal/v371/n6496/abs/371408a0.html.

Linde, A. T. & Sacks, I. S., 1998. Triggering of volcanic eruptions. *Nature*, 395(October), pp.272–275.

Llewellin, E. W., Mader, H. M. & Wilson, S. D. R., 2016. The rheology of a bubbly liquid. *Mathematical, Physical & Engineering Sciences*, 458(2020), pp.987–1016.

Llewellin, E. W. & Manga, M., 2005. Bubble suspension rheology and implications for conduit flow. *Journal of Volcanology and Geothermal Research*, 143, pp.205–217.

Lyon, B., 2016. Spreading of non-Newtonian fluids. , (July).

Mader, H. M., Llewellin, E. W. & Mueller, S. P., 2013. The rheology of two-phase magmas : A review and analysis. *Journal of Volcanology and Geothermal Research*, 257, pp.135–158.

Available at: http://dx.doi.org/10.1016/j.jvolgeores.2013.02.014.

Manga, M. & Brodsky, E., 2006. Seismic triggering of eruptions in the far field: volcanoes and geysers. *Annual Review of Earth and Planetary Sciences*, 34(1), pp.263–291.

Manga, M., Brumm, M. & Rudolph, M. L., 2009. Earthquake triggering of mud volcanoes. *Marine and Petroleum Geology*, 26(9), pp.1785–1798.

Marzocchi, W., 2002. Remote seismic influence on large explosive eruptions. *Journal of Geophysical Research*, 107(September 2000), pp.1–7.

Marzocchi, W., Scandone, R. & Mulargia, F., 1993. The tectonic setting of Mount Vesuvius and the correlation between its eruptions and the earthquakes of the Southern Apennines. *Journal of Volcanology and Geothermal Research*, 58(1–4), pp.27–41. Available at: http://www.sciencedirect.com/science/article/pii/0377027393901006.

Mathieu, L. van Wyk de Vries, B., Holohan, E. P., Troll, V. R., 2008. *Dykes, cups, saucers and sills: Analogue experiments on magma intrusion into brittle rocks*, 271(1-13).

Mcintosh, I.M. Llewellin, E. W., Humphreys, M. C. S., Nichols, A. R. L., Burgisser, A., Schipper, C. I., Larsen, J F., 2014. Distribution of dissolved water in magmatic glass records growth and resorption of bubbles. *Earth and Planetary Science Letters*, 401, pp.1–11. Available at: http://dx.doi.org/10.1016/j.epsl.2014.05.037.

Meijering, E., Dzyubachyk, O. & Smal, I., 2012. Methods for cell and particle tracking. *Methods Enzymol*, 504(9), pp.183–200. Available at: http://www.ncbi.nlm.nih.gov/pubmed/22264535.

Merle, O., 2015. The scaling of experiments on volcanic systems. *Frontiers in Earth Sciences*, 3(June), pp.1–15.

Murphy, J. R. & O'Brien, L. J., 1977. The correlation of peak ground acceleration amplitude with seismic intensity and other physical parameters acceleration. *Bulletin of the Seismological Society of America*, 67(3), pp.877–915.

Nakayama, Y. Boucher, R. F., 1998. 9 – Drag and lift. In *Introduction to Fluid Mechanics*. pp. 148–170.

Namiki, A. Rivalta, E., Woith, H., Walter, T. R., 2016. Sloshing of a bubbly magma reservoir as a mechanism of triggered eruptions. *Jorunal of Volcanology and Geothermal Research*, 320, pp.156–171.

Namiki, A. & Manga, M., 2006. Influence of decompression rate on the expansion velocity and expansion style of bubbly fluids. *Journal of Geophysical Research: Solid Earth*, 111(11), pp.1–17.

Namiki, A. & Manga, M., 2005. Response of a bubble bearing viscoelastic fluid to rapid decompression: Implications for explosive volcanic eruptions. *Earth and Planetary Science Letters*, 236(1–2), pp.269–284.

Naumov, V.B. Kovalenko, V. I., Dorofeeva, V. A., Girnis, A. V., Yarmolyuk, V. V., 2010. Average compositions of igneous melts from main geodynamic settings according to the investigation of melt inclusions. *Geochamistry International*, 48(12), pp.1266–1288.

Obermier, 2015. KORASILON Fluids M. , pp.1–10.

Parfitt, L. & Wilson, L., 2009. *Fundamentals of Physical Volcanology* 1st ed., Malden, MA: Blackwell Publishing. Available at: https://books.google.co.nz/books?id=ptpCiNkwLj8C.

Parmigiani, A., Faroughi, S., Huber, C., Bachmann, O., Su, Y., 2016. Bubble accumulation and its role in the evolution of magma reservoirs in the upper crust. *Nature*, 532(7600), pp.492–495. Available at: http://www.nature.com/doifinder/10.1038/nature17401.

Pettinga, J. R., 2003. Mud volcano eruption within the emergent accretionary Hikurangi margin, southern Hawke's Bay, New Zealand. *New Zealand Journal of Geology and Geophysics*, 46(1), pp.107–121. Available at: http://dx.doi.org/10.1080/00288306.2003.9514999.

Plesset, M. S. & Prosperetti, A., 1977. Bubble dynamics and cavitation. *Annual Review of Fluid Mechanics*, 9, pp.145–185.

Pyle, D. M. & Pyle, D. L., 1995. Bubble migration and the initiation of volcanic eruptions. *Journal of Volcanology and Geothermal Research*, 67(4), pp.227–232.

Rasband, W.S., 2015. ImageJ. Available at: http://imagej.nih.gov/ij.

Rivalta, E. & Dahm, T., 2006. Acceleration of buoyancy-driven fractures and magmatic dikes beneath the free surface. *Geophysical Journal International* , 166(3), pp.1424–1439. Available at: http://gji.oxfordjournals.org/content/166/3/1424.abstract.

Roeloffs, E. A., 1998. Persistent water level changes in a well near Parkfield, California, due to local and distant earthquakes. *Journal of Geophysical Research: Solid Earth*, 103(B1), pp.869–889. Available at: http:https://dx.doi.org/10.1029/97JB02335.

Roman, D. C. & Cashman, K. V., 2006. The origin of volcano-tectonic earthquake swarms. *Geology*, 34(6), pp.457–460.

Rust, A. C., Manga, M. & Cashman, K. V., 2003. Determining flow type, shear rate and shear stress in magmas from bubble shapes and orientations. *Journal of Volcanology and Geothermal Research*, 122(1–2), pp.111–132.

Sahagian, D. L., 1993. More bubbles in volcanic systems. *Nature*, 361(6410), pp.308–308.

Sahagian, D. L. & Proussevitch, A. A., 1992. Bubbles in Volcanic Systems. *Nature*, 395(6395), pp.485–485.

Salmon, M. W., Short, S. A. & Kennedy, R. P., 1992. Strong motion duration and earthquake magnitude relationships.

Sánchez, C. et al., 2014. Experimental modeling of infrasound emission from slug bursting on volcanoes. *Geophysical Research Letters*, 41(19), pp.6705–6711. Available at: http://doi.wiley.com/10.1002/2014GL061068 [Accessed January 19, 2017].

Sánchez, J. J. & McNutt, S. R., 2004. Intermediate-term declines in seismicity at Mt. Wrangell and Mt. Veniaminof Volcanoes, Alaska, following the 3 November 2002 M w 7.9 Denali fault earthquake. *Bulletin of the Seismological Society of America*, 94(6B), pp.S370–S383.

Schapery, R. A., 1969. On the characterization of nonlinear viscoelastic materials. *Polymer Engineering and Science*, 9(4), pp.295–310. Available at: http://doi.wiley.com/10.1002/pen.760090410 [Accessed February 14, 2017].

Segal, V., 2002. Severe plastic deformation: simple shear versus pure shear. *Materials Science and Engineering: A*, 338(1), pp.331–344.

Sheth, H., 2014. What drives centuries-long polygenetic scoria cone activity at Barren Island volcano? *Journal of Volcanology and Geothermal Research*, 289, pp.64–80.

Sigurdsson, H., 2000. *Encyclopedia of volcanoes*,

Sørensen, M. B., Atakan, K. & Pulido, N., 2007. Simulated strong ground motions for the great M 9.3 Sumatra-Andaman earthquake of 26 December 2004. *Bulletin of the Seismological Society of America*, 97(1 A SUPPL.), pp.139–151.

Spina, L., Cimarelli, C., Scheu, B., Di Genova, D., Dingwell, D. B., 2016. *On the slow decompressive response of volatile- and crystal-bearing magmas: An analogue experimental investigation*, 433(44-53).

Steinberg, G. S., Steinberg, A. S. & Merzhanov, A. G., 1989. Fluid mechanism of pressure growth in volcanic (magamtic) systems. *Modern Geology*, 13, pp.257–266.

Taddeucci, J., Spieler, O., Ichihara, M., Dingwell, D., Scarlato, P., 2006. Flow and fracturing of viscoelastic media under diffusion-driven bubble growth: An analogue experiment for eruptive volcanic conduits. *Earth and Planetary Science Letters*, 243(3–4), pp.771–785. Available at: http://linkinghub.elsevier.com/retrieve/pii/S0012821X06000306.

Tait, S., Jaupart, C. & Vergniolle, S., 1989. Pressure, gas content and eruption periodicity of a shallow, crystallising magma chamber. *Earth and Planetary Science Letters*, 92, pp.107–123.

Takeuchi, S., 2015. A melt viscosity scale for preeruptive magmas. *Bulletin of Volcanology*, 77(5), pp.1–11. Available at: http://link.springer.com/10.1007/s00445-015-0929-8.

Talaia, M. A. R., 2007. Terminal Velocity of a Bubble Rise in a Liquid Column. *Engineering and Technology*, 28(5), pp.264–268.

Trifunac, M. D. & Brady, A. G., 1975. A study on the duration of strong earthquake ground motion. *Bulletin of the Seismological Society of America*, 65(3), pp.581–626. Available at: http://www.bssaonline.org/content/65/3/581.abstract.

Troll, V. R., Deegan, F. M., Jolis, Ester M., Budd, D. A., Dahren, B., Schwarzkopf, L. M., 2015. Ancient Oral Tradition Describes Volcano-Earthquake Interaction at Merapi Volcano, Indonesia. *Geografiska Annaler: Series A, Physical Geography*, 97(1), pp.137–166. Available at: http://doi.wiley.com/10.1111/geoa.12099 [Accessed January 18, 2017].

Ukawa, M., 2005. Deep low-frequency earthquake swarm in the mid crust beneath Mount Fuji (Japan) in 2000 and 2001. *Bulletin of Volcanology*, 68(1), pp.47–56.

Unglert, K. & Jellinek, A. M., 2015. Volcanic tremor and frequency gliding during dike intrusions at Kilauea: A tale of three eruptions. *Journal of Geophysical Research B: Solid Earth*, 120(2), pp.1142–1158.

USGS, 2016. USGS ShakeMap: Conception, Chile. *USGS*. Available at: https://earthquake.usgs.gov/earthquakes/eventpage/official19600522191120_30#shakemap [Accessed February 7, 2017].

Vidal, V., Ripepe, M., Divoux, T., Legrand, D., Géminard, J. C., Melo, F., 2010. Dynamics of soap bubble bursting and its implications to volcano acoustics. *Geophysical Research Letters*, 37(7), pp.1–4.

Villalobos, F., 2011. Crustal deformation associated with the 1960 earthquake events in the south of Chile. In *5th International Conference on Earthquake Geotechnical Engineering*. Available at: http://civil.ucsc.cl/investigacion/fvillalobos/2010_5ICEGE_A.pdf.

De Vivo, B., Lima, A. & Webster, J. D., 2005. Volatiles in Magmatic-Volcanic Systems. *Elements*, 1(1), pp.19–24. Available at: http://elements.geoscienceworld.org/cgi/content/abstract/1/1/19.

Wald, J. David; Quitoriano, V., Heaton, H., Kanamori, H., 1999. Relationships between peak ground acceleration, peak ground velocity, and modified mercalli intensity in California. *Earthquake Spectra*, 15(3), pp.557–564.

Walter, T. R., 2007. How a tectonic earthquake may wake up volcanoes: Stress transfer during the 1996 earthquake-eruption sequence at the Karymsky Volcanic Group, Kamchatka. *Earth and Planetary Science Letters*, 264, pp.347–359.

Walter, T. R. Wang, R., Acocella, V., Neri, M., Grosser, H., Zschau, J., 2009. Simultaneous magma and gas eruptions at three volcanoes in southern Italy: An earthquake trigger? *Geology*, 37(3), pp.251–254.

Walter, T. R. Wang, R., Zimmer, M., Grosser, H., Lühr, B., Ratdomopurbo, A., 2007. Volcanic activity influenced by tectonic earthquakes: Static and dynamic stress triggering at Mt. Merapi. *Geophysical Research Letters*, 34(5), pp.1–5.

Walter, T. R. & Amelung, F., 2007. Volcanic eruptions following Mw 9 megathrust earthquakes: Implications of the Sumatra-Andaman volcanoes. *Geology*, 35(6), pp.539–542.

Walter, T. R. & Amelung, F., 2006. Volcano-earthquake interaction at Mauna Loa volcano, Hawaii. *Journal of Geophysical Research: Solid Earth*, 111(5), pp.1–17.

Wang, F. Shen, Z., Wang, Y., Wang, M., 2011. Influence of the March 11, 2011 M w 9.0 Tohoku-oki earthquake on regional volcanic activities. *Chinese Science Bulletin*, 56(20), pp.2077–2081.

Watt, S. F. L., Pyle, D. M. & Mather, T. A., 2009. The influence of great earthquakes on volcanic eruption rate along the Chilean subduction zone. *Earth and Planetary Science Letters*, 277(3–4), pp.399–407. Available at: http://www.sciencedirect.com/science/article/B6V61-4V4M2YX-1/2/0cc6b4347ff33f8e4c41b970a9d149c6.

Weischet, W., 1963. Further observations of geologic and geomorphic changes resulting from the catastrophic earthquake of May 1960, in Chile. *Bulletin of the Seismological Society of America*, 53(6), pp.1237–1257. Available at: http://www.bssaonline.org/content/53/6/1237.abstract.

Xin, L., Tangyong, G., Jiening, X., Tong, Z., Wei, Z., Shipeng, L., 2014. A new type seismic intensity meter. *Geodesy and Geodynamics*, 5(4), pp.73–78.

Yoshimura, S. & Nakamura, M., 2008. Diffusive dehydration and bubble resorption during open-system degassing of rhyolitic melts. *Journal of Volcanology and Geothermal Research*, 178(1), pp.72–80.

11. Appendix

Table 7. Full experimental parameters and results of the experiments. The lowest difference in rise velocity is highlighted in blue and the highest is highlighted red.

Experiment Parameter	Frequency (Hz)	Displacement (mm)	Acceleration (g)	Bubble size (mm)	Viscosity (Pa s)	Still rise velocity (cm/minute)	Shaking ride velocity	Diff (%)
E6	3	20	0.43	15	2000	0.4910	0.5363	9.23%
E7	1	120	0.33	15	2000	0.4910	0.5288	7.69%
E8	2	120	0.95	15	2000	0.4910	0.5479	11.60%
E9	1.6	160	0.95	15	2000	0.4910	0.5186	5.62%
E10	4	20	0.73	15	2000	0.4910	0.5091	3.69%
E11	1.6	160	0.94	15	2000	0.4910	0.5145	4.79%
E5	1	20	0.12	20	2000	0.9385	0.9935	5.86%
E6	3	20	0.43	20	2000	0.9385	0.9739	3.77%
E7	1	120	0.33	20	2000	0.9385	1.0064	7.24%
E8	2	120	0.95	20	2000	0.9385	1.0475	11.61%
E9	1.6	160	0.95	20	2000	0.9385	0.9827	4.71%
E10	4	20	0.73	20	2000	0.9385	0.9913	5.62%
E11	1.6	160	0.94	20	2000	0.9385	1.0344	10.21%
E5	1	20	0.12	25	2000	1.3905	1.4283	2.72%
E6	3	20	0.43	25	2000	1.3905	1.4761	6.16%
E7	1	120	0.33	25	2000	1.3905	1.4170	1.91%
E8	2	120	0.95	25	2000	1.3905	1.5485	11.37%
E9	1.6	160	0.95	25	2000	1.3905	1.4279	2.69%
E10	4	20	0.73	25	2000	1.3905	1.4266	2.60%
E11	1.6	160	0.94	25	2000	1.3905	1.4589	4.92%
E6	3	20	0.43	15	10000	0.1133	0.1201	6.01%
E7	1	120	0.33	15	10000	0.1133	0.1205	6.42%
E8	2	120	0.95	15	10000	0.1133	0.1257	10.96%
E9	1.6	160	0.95	15	10000	0.1133	0.1202	6.08%
E10	4	20	0.73	15	10000	0.1133	0.1192	5.27%
E11	1.6	160	0.94	15	10000	0.1133	0.1212	7.00%
E5	1	20	0.12	20	10000	0.1900	0.1965	3.40%
E6	3	20	0.43	20	10000	0.1900	0.1967	3.54%
E7	1	120	0.33	20	10000	0.1900	0.1993	4.88%
E8	2	120	0.95	20	10000	0.1900	0.2153	13.33%
E9	1.6	160	0.95	20	10000	0.1900	0.2043	7.53%
E10	4	20	0.73	20	10000	0.1900	0.1976	3.98%
E11	1.6	160	0.94	20	10000	0.1900	0.2067	8.76%
E5	1	20	0.12	25	10000	0.2798	0.2890	3.29%
E6	3	20	0.43	25	10000	0.2798	0.2911	4.06%
E7	1	120	0.33	25	10000	0.2798	0.2990	6.87%
E8	2	120	0.95	25	10000	0.2798	0.3021	8.00%
E9	1.6	160	0.95	25	10000	0.2798	0.3005	7.40%
E10	4	20	0.73	25	10000	0.2798	0.2986	6.72%
E11	1.6	160	0.94	25	10000	0.2798	0.2994	7.02%

E6	3	20	0.43	15	30000	0.0385	0.0408	6.01%
E7	1	120	0.33	15	30000	0.0385	0.0408	6.01%
E8	2	120	0.95	15	30000	0.0385	0.0435	12.95%
E9	1.6	160	0.95	15	30000	0.0385	0.0407	5.67%
E10	4	20	0.73	15	30000	0.0385	0.0401	4.07%
E11	1.6	160	0.94	15	30000	0.0385	0.0401	4.07%
E5	1	20	0.12	20	30000	0.0569	0.0601	5.58%
E6	3	20	0.43	20	30000	0.0569	0.0609	6.87%
E7	1	120	0.33	20	30000	0.0569	0.0587	3.00%
E8	2	120	0.95	20	30000	0.0569	0.0613	7.71%
E9	1.6	160	0.95	20	30000	0.0569	0.0604	6.01%
E10	4	20	0.73	20	30000	0.0569	0.0582	2.12%
E11	1.6	160	0.94	20	30000	0.0569	0.0593	4.13%
E5	1	20	0.12	25	30000	0.0906	0.0949	4.73%
E6	3	20	0.43	25	30000	0.0906	0.0967	6.70%
E7	1	120	0.33	25	30000	0.0906	0.0941	3.90%
E8	2	120	0.95	25	30000	0.0906	0.0999	10.30%
E9	1.6	160	0.95	25	30000	0.0906	0.0943	4.14%
E10	4	20	0.73	25	30000	0.0906	0.0953	5.21%
E11	1.6	160	0.94	25	30000	0.0906	0.0979	8.12%